Dalton Transactions

How hydrothermal synthesis improves the preparation of $(Zr,Ce)SiO_4$ solid solutions

Journal:	*Dalton Transactions*
Manuscript ID	DT-ART-05-2023-001524.R2
Article Type:	Paper
Date Submitted by the Author:	20-Jun-2023

Complete List of Authors:	Barral, Thomas; CEA Marcoule, ICSM, Univ Montpellier, CNRS, CEA, ENSCM Estevenon, Paul; CEA Marcoule, CEA, DES, ISEC, DMRC, Univ Montpellier Chanteau, Yann; CEA Marcoule, ICSM, Univ Montpellier, CNRS, CEA, ENSCM Kaczmarek, Thibault; CEA Marcoule, ICSM, Univ Montpellier, CNRS, CEA, ENSCM Strzelecki, Andrew; Washington State University, Chemistry; Washington State University, School of Mechanical and Materials Engineering; Los Alamos National Laboratory, Earth and Environmental Science Division Menut, Denis; SOLEIL, Welcomme, Eleonore; CEA Marcoule, CEA, DES, ISEC, DMRC, Univ Montpellier Szenknect, Stéphanie; CEA Marcoule, ICSM, Univ Montpellier, CNRS, CEA, ENSCM Moisy, Philippe; CEA Marcoule, CEA, DES, ISEC, DMRC, Univ Montpellier Guo, Xiaofeng; Washington State University, Chemistry; Washington State University, School of Mechanical and Materials Engineering Dacheux, Nicolas; University of Montpellier, ICSM, CEA, CNRS, ENSCM, Univ Montpellier

How hydrothermal synthesis improves the synthesis of $(Zr,Ce)SiO_4$ solid solutions

Thomas Barral[1], Paul Estevenon[2], Yann Chanteau[1], Thibault Kaczmarek[1,2], Andrew C. Strzelecki[3,4,5], Denis Menut[6], Eleonore Welcomme[2], Stephanie Szenknect[1], Philippe Moisy[2], Xiaofeng Guo[3,4], Nicolas Dacheux[1,*]

[1] ICSM, Univ Montpellier, CNRS, CEA, ENSCM, Bagnols-sur-Cèze, France

[2] CEA, DES, ISEC, DMRC, Univ Montpellier, Marcoule, France.

[3] Department of Chemistry, Washington State University, Pullman, Washington 99164, United States

[4] School of Mechanical and Materials Engineering, Washington State University, Pullman, Washington 99164, United States

[5] Earth and Environmental Sciences Division, Los Alamos National Laboratory, P.O. Box 1663, Los Alamos, NM 87545, USA

[6] Synchrotron SOLEIL, L'Orme des Merisiers, Départementale 128, 91190 Saint Aubin, France

ABSTRACT:

Although $ZrSiO_4$ is the most well-known compound in the zircon-structured family (space group $I4_1/amd$), the experimental conditions for preparing pure and well-crystallized phases which are doped with a tetravalent element via hydrothermal synthesis has never been clearly discussed in the literature. With the aim to answer this question, the experimental conditions of preparation of $ZrSiO_4$ and $(Zr,Ce)SiO_4$ were investigated in order to synthesize well-crystallized and pure phases. A multiparametric study has been carried out using soft hydrothermal conditions, with variables including reactant concentration, initial pH of the reactive medium, and duration of the hydrothermal treatment. Pure $ZrSiO_4$ was obtained through hydrothermal treatment for 7 days at 250°C, within a large acidity range ($1.0 \leq pH \leq 9.0$) and starting from $C_{Si} \approx C_{Zr} \geq 0.2$ M. As hydrothermally prepared zircon structured phases can be both hydrated and hydroxylated, its annealed form was also studied after heating to 1000°C. Based on these results, the synthesis of $(Zr,Ce)SiO_4$ solid solutions were also investigated. The optimal hydrothermal conditions to acquire pure and crystallized phases were obtained in 7 days at 250°C with initial pH = 1 and concentration of the reactants equal to 0.2 $mol \cdot L^{-1}$. This led to $Zr_{1-x}Ce_xSiO_4$ solid solutions with the incorporated Ce content up to 40 mol.%. Samples were characterized by multiple methods, including lab and synchrotron PXRD, IR and Raman spectroscopies, SEM, and TGA. Moreover, it was found that these phases were thermally stable in air up to at least 1000°C.

KEYWORDS: zircon, silicate, wet chemistry route, hydrothermal synthesis

1. INTRODUCTION

Although the hydrothermal synthesis of the zircon group (space group $I4_1/amd$ [1], **Figure 1**) silicates has long been known, with the first hydrothermal synthesis of $ZrSiO_4$ carried out by Von Chrustchoff in 1892 [2], their preparation continues to arouse a great interest, in particular the preparation solid solutions. Nature has long derived zircon structured silicates, in the form of minerals, which exhibit a plethora of solid solutions in both crystallographic sites. The compositional end-members of these minerals include, zircon ($ZrSiO_4$), hafnon ($HfSiO_4$), stetindite ($CeSiO_4$), thorite ($ThSiO_4$), and coffinite ($USiO_4$), which can form either in primary igneous (i.e., magmatic) or secondary hydrothermal (i.e., epithermal) depositional environments. Elements which can form zircon-type solid solution in the dodecahedral site (M-site) tend to be high-field strength elements, including group III (Sc and Y), group IV (Ti, Zr, and Hf), lanthanides (Ln, La – Lu), and early actinides (An, Ac – Pu). Anthropogenic conditions have also led to the formation of solid solutions with a zircon-type structure, with $(Zr,An)SiO_4$, being observed in corium lavas coming from Chernobyl nuclear accident [3], [4]. Moreover, as a part of Fukushima Daichi nuclear core contained MOx fuels, the presence of $(Zr,Pu)SiO_4$ phases in the corium lavas has been suggested [5]. Understanding properties of such solid solutions is thus crucial for predicting the behavior of corium in the case of severe accident as well as for the determination of remediation methods in such accidental situations. On the other hand, because of the highly refractory character of zircon-type materials to dissolution, the use of $(Zr,An)SiO_4$ solid solutions has been considered as a potential radwaste matrix for the long-term storage of actinides [6]–[8]. A complete description of zircon-based solid solutions is thus mandatory to improve our understanding of how zircon phases form in lavas during a nuclear accident or how they behave in the long-term storage of dismantled nuclear weapons in a geological repository [7], [8].

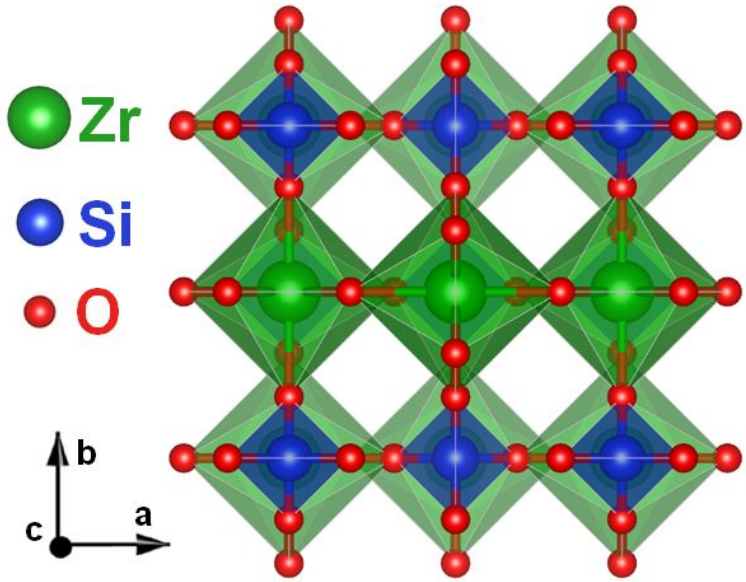

Figure 1. Projection of the zircon ($ZrSiO_4$) structure down the c-axis according to Finch *et al.* [1].

While the synthesis of pure silicate end-members of the zircon group $MSiO_4$ (with M = Zr, Ce, Hf, Th, Pa, U, Np, Pu, Am) [2], [9]–[14], and a few solid solutions, including $(Zr,Hf)SiO_4$ [15]–[17][18] and $(Th,U)SiO_4$ [19]–[23], a significant knowledge gap still remains in the scientific literature on the preparation of several solid solution systems. This is demonstrated by that synthetic $(Zr,An)SiO_4$ and $(Zr,Ce)SiO_4$ solid solutions appear to be much more difficult [24]–[27][28]. Indeed, the syntheses by dry chemical processes did not allow to produce solid solutions with high concentration An/Ce incorporation rates in the zircon host matrix. This can be explained by the difference in terms of ionic radius between Zr^{4+} and Ce^{4+}/An^{4+} ions in the eight coordination (Zr = 0.84 Å, Ce = 0.97 Å, Th = 1.05 Å, Pa = 1.01 Å, U = 1.00 Å, Np = 0.98 Å, Pu = 0.96 Å and Am = 0.95 Å, respectively) [29], resulting in strong distortion of the zircon lattice. Thus, the solubility limits of actinides in the zircon structure using solid-state synthesis were found to be low (7–10 wt.%, 7 ± 1 wt.%; 4 ± 1 wt.% and 2 ± 1 wt.% for Pu, Ce, U and Th, respectively) [24], [30], [31]. However, such dry route syntheses did not allow the formation of solid solutions as rich as that formed in the corium lavas for $(Zr,U)SiO_4$ (up to 12.9 wt.%) [3]. Finally, simulations performed on the thermodynamic properties of such solid solutions have shown that actinide-enriched solid solutions are enthalpically metastable [27], [32], [33], which however, contradicts to experimental calorimetry results [22], [23].

Several studies were recently carried out by Estevenon *et al*. on the hydrothermal synthesis of zircon-type silicates ($HfSiO_4$, $CeSiO_4$, $ThSiO_4$, and $PuSiO_4$) and contributed to major advances in the understanding of these synthetic routes [10]–[13], [34], [35]. The aim of this work is to take advantage of this recent knowledge in order to develop the synthesis of $(Zr,Ce)SiO_4$ solid solutions with higher concentrations (mol.%) of Ce than already reported [24], [25]. This solid solution system was selected on the basis that Ce is often viewed as a non-radioactive analog of Pu due to their similarity in physico-chemical properties (i.e., ionic radii and hydrolysis constants) [29], [36]–[38]. Therefore, through understanding the synthetic conditions of $(Zr,Ce)SiO_4$ solid solution one can gain important insight towards synthesizing $(Zr,Pu)SiO_4$ solid solution with high mol.% Pu, further allowing for the derivation of thermodynamic parameters.

2. MATERIALS AND METHODS

2.1. Syntheses

2.1.1. Preparation of stetindite $CeSiO_4$

Stetindite ($CeSiO_4$) sample was synthesized by hydrothermal method from Ce(III)-silicate solid precursor (A-$Ce_2Si_2O_7$), slightly adapting the protocol recently developed by Estevenon *et al*. [10]. A mixture containing 1.5 g of CeO_2 (Sigma Aldrich, particle size < 5 µm) and 0.571 g of SiO_2 (Sigma Aldrich, 10-20 nm) was mechanically milled (30 Hz, 1 hour) in a Retsch MM 200 vibration mill mixer apparatus using a tungsten carbide milling jar. In this mixture, a silicate excess of 9 mol.% was thus considered to ensure the formation of the silicate phase. This mixture was pelletized by uniaxial pressing (500 MPa) at room temperature and then heated at 1350 °C for 9 hours under reducing atmosphere (Ar–4% H_2) to form the Ce(III)-silicate solid precursor, A-$Ce_2Si_2O_7$ (space group: $P4_1$). In a 23 mL Teflon lined Parr reactor, 200 mg of A-$Ce_2Si_2O_7$ was put in contact with 4 mL of 0.75 mol·L^{-1} HNO_3 solution (prepared by dilution of ACS grade 70% HNO_3, Sigma Aldrich). Moreover, an additional excess of 8 mol.% of silicate was introduced to the solution as $Na_2SiO_3 \cdot 5H_2O$ (8.8 mg) in order to avoid the formation of CeO_2. The pH of the solution was then adjusted to 6.5 ± 0.1 with a freshly prepared 8 mol·L^{-1} NaOH solution (from ACS grade NaOH pellets, Sigma Aldrich). This mixture was then hydrothermally treated for 7 days at 150°C under air atmosphere using a Parr autoclave (Parr 4749 acid digestion vessel). After cooling, the final solid was separated from the supernatant solution by centrifugation at 12 000 rpm, washed twice with deionized water and once with ethanol and finally dried overnight in an oven at 60°C.

2.1.2. Preparation of zircon : $ZrSiO_4$

The preparation of zircon was inspired from the protocols described by Valero [39] and by Estevenon et al. for the $HfSiO_4$ synthesis [11], [12]. $Na_2SiO_3 \cdot 5H_2O$ (Sigma-Aldrich, ≥ 95%) and $ZrO(NO_3)_2 \cdot 2H_2O$ (Sigma-Aldrich, ≥ 99%) were mixed together with a 5 mol.% silicate excess and dissolved in 1 mol·L^{-1} HNO_3 solution (prepared by dilution of Sigma Aldrich ACS grade solution of 70% HNO_3). The pH was then adjusted to the expected value thanks to a freshly prepared 8 mol·L^{-1} NaOH solution (obtained from Sigma Aldrich ACS grade 98 % NaOH).

All of the prepared mixtures were introduced in 23 mL Teflon lined containers. The containers were put in Parr autoclaves (Parr 4749) then placed in an oven to reach hydrothermal

conditions at 250°C under autogenous pressure for varying holding times. The final cooling to room temperature was done within one hour. Then, the precipitates were separated from the supernatants by centrifugation for 12 min at 12 000 rpm, washed twice with deionized water and once with ethanol, and finally dried overnight in an oven at 60°C.

2.1.3. Preparation of $(Zr,Ce)SiO_4$ solid solutions

All of the reagents used were supplied by Sigma-Aldrich. $Na_2SiO_3 \cdot 5H_2O$ ($\geq 95\%$), $ZrO(NO_3)_2 \cdot 2H_2O$ ($\geq 99\%$) and $(NH_4)_2Ce(NO_3)_6$ ($\geq 98.5\%$) were used as aqueous silicate, zirconium and cerium precursors respectively. A 1 $mol \cdot L^{-1}$ HNO_3 solution was prepared by dilution of Sigma Aldrich ACS grade solution of 70% HNO_3. A 8 $mol \cdot L^{-1}$ NaOH solution was freshly prepared from Sigma Aldrich ACS grade NaOH (98 %) before the experiments.

The syntheses of $(Zr,Ce)SiO_4$ solid solutions were performed on the basis of the conditions previously determined for each end-member, $CeSiO_4$ and $ZrSiO_4$, described above. Aqueous zirconium, cerium and silicate solutions were prepared by dissolving $ZrO(NO_3)_2 \cdot 2H_2O$, $(NH_4)_2Ce(NO_3)_6$ and $Na_2SiO_3.5H_2O$ in 1 $mol \cdot L^{-1}$ HNO_3 in order to obtain a reacting mixture with a silicate excess of 5 mol.%, aiming at obtaining Zr and Ce oxide-free samples. The global cation concentration ($C_{Zr(IV)} + C_{Ce(IV)}$) was set to 0.2 $mol \cdot L^{-1}$ with varying zirconium and cerium concentrations depending on the targeted composition. The pH of the mixture was then adjusted to about pH = 1 with the help of 8 $mol \cdot L^{-1}$ NaOH.

All of the prepared mixtures were introduced in 23 mL Teflon lined containers (Parr 4749). The conditions of the hydrothermal treatment were fixed to t = 7 days and T = 250°C, under autogenous pressure. The final cooling to room temperature was done within one hour. Then, the precipitates were separated from the supernatants by centrifugation at 12 000 rpm for 12 min, washed twice with deionized water and once with ethanol, and finally dried overnight at 60°C in an oven. Some of the obtained powders were finally annealed at 1000°C in a muffle furnace for 10 hours.

2.2. Characterization of the prepared samples

PXRD data were collected on the resulting powders using the Bruker D8 advance diffractometer equipped with a LynxEye detector and using Cu Kα radiation (λ = 1.54184 Å) in a reflection geometry (parallel beam). Patterns were recorded between 5° and 90° (2θ) with steps of 0.019° and a total counting time of 2.5 to 3 hours per sample. Pure silicon was used as

a standard material to extract the instrumental function. Then, the collected data were refined by the Rietveld method using the Fullprof suite package [40]. During the refinements, different profile and structure parameters were allowed to vary, such as the zero shift, unit cell parameters, scale factor, and overall displacement factor. However, the occupancy of each site was fixed to the calculated values. In order to facilitate the comparison of diffractograms, the background has been subtracted and the intensity divided by the maximum.

In order to ensure the identification of all of the phases present in annealed samples (especially to avoid the misidentification of secondary oxide phases), High Resolution Powder X-Ray Diffraction have been performed at the MARS beamline of the SOLEIL Synchrotron on the dedicated CX2 end-station. The CX2 end-station is equipped with a four-circle diffractometer that we used in transmission mode. Before being collected by a set of 24 scintillation detectors, the X-ray beams diffracted by the samples are highly collimated using a multi-crystal analyzer stage made of two banks of Ge(111) analyzer crystals mounted on the 2θ arm. Diffraction patterns were obtained after the normalization of the diffraction signals coming from all the 24 detectors. This signal normalization was done using a specific procedure developed by the beamline [41]. It is well-known that this geometry associated with a capillary sample holder is one of the most efficient ways to record very high-resolution diffraction patterns. The samples were placed in 0.6 mm Kapton capillary tubes (1.5 cm long). The powder was sealed in the tube by epoxy resin. The detector geometry parameters were calibrated using the NIST standard LaB_6 (SRM 660b). The HR-XRD end-station was set at 17.0 keV ($\lambda = 0.72959$ Å) after calibration at the yttrium K-edge energy (E = 17.038 keV) with an incident collimated X-ray beam sizing about 300 × 1000 μm² (V × H). Samples were spun in the incoming X-ray beam to average a potential texturing effect. XRD patterns were collected in the 0 to 115° 2θ range, with an angular step of 0.002° and a counting time of 0.1 s per frame in a continuous scan mode. Data were treated using the TOPAS software [42]. XRD pattern fitting was done using Le Bail model, considering no sample texture, no strain, and the structure factors given by the atomic standard.

Raman spectra were recorded with a Horiba-Jobin Yvon Aramis device equipped with an edge filter and a Nd:YAG laser (532 nm) that delivered 60 mW at the sample surface. In order to avoid any laser-induced degradation of the compound, the power was turned down by the means of optical filters. The laser beam was then focused on the sample using an Olympus BX 41 microscope with an × 50LMP objective, resulting in a spot area of ~1 μm^2 and a power of 39 mW. For each spectrum, measurements were performed in the 100–4000 cm^{-1} range for

dwell time of 1 to 30 s. Four scans were recorded and averaged for each analyzed area in order to minimize the instrumental error. In order to facilitate their comparison, the spectra were normalized in the [0–1] range.

FTIR spectra were recorded with a Perkin-Elmer FTIR Spectrum 100 device in the 300 – 4000 cm^{-1} range. Powdered samples were deposited on the surface of an ATR crystal without any prior preparation. The spectra collected in such operating conditions exhibited a resolution lower than 4 cm^{-1}. Five scans were performed and merged for each sample to average the instrumental error. To facilitate their comparison, the spectra were divided by their maximum intensity.

SEM observations were directly conducted using a FEI Quanta 200 electronic microscope on small, powdered samples without any prior preparation such as metallization. The electronic microscope was equipped either with an Everhart-Thornley Detector (ETD) or a Back-Scattered Electron Detector (BSED), under high vacuum conditions with a low accelerating voltage (2 kV). These conditions were chosen to create a beam deceleration effect that allowed the collection of high-resolution images.

Thermogravimetric analyses measurements were conducted on Mettler Toledo TGA/DSC 3+ apparatus. After recording a baseline using an empty alumina crucible, about 20 mg of powdered sample were placed into another alumina crucible of the same type, then weight loss was measured during a heat treatment up to 1000 °C with a rate of 5°C·min^{-1} under air. The hydration level of the prepared samples prior calcination was thus determined.

3. RESULTS AND DISCUSSION

3.1. Optimization of the zircon $ZrSiO_4$ preparation

Even if the hydrothermal synthesis of $ZrSiO_4$ was often mentioned in the literature [31], [39], [43]–[50], [51]–[55], there are still an important details concerning the description of the optimal experimental conditions which are often lacking. Overall, the formation of $ZrSiO_4$ under hydrothermal conditions, even if always successful, is known to be slow, leading to poorly crystallized samples. Additionally, the impact of crucial parameters known to affect the synthesis of chemical analogues $MSiO_4$ (M = Hf, Ce, Th, U, Pu), such as the initial pH, the reagent concentrations and the hydrothermal treatment duration has never been evaluated. Temperature was fixed to 250°C as, according to literature [11], [12], [39], [43], [45], its only role was to increase the reaction kinetics.

3.1.1. Effect of the pH of the starting solution

Considering a starting mixture with Zr concentration of 0.2 mol·L^{-1} and a Si/Zr molar ratio of 1.05, the effect of the pH of the starting mixture on the nature of the resulting precipitate was followed between 1.0 mol·L^{-1} HNO_3 and pH_{ini} = 11.7. Hydrothermal treatments were performed at 250°C for 20 days to limit the constraints related to the crystallization kinetics of $ZrSiO_4$. The whole set of the samples prepared over the studied initial pH range were characterized by PXRD (**Figure 2**).

From these results, $ZrSiO_4$ was formed on a wide range of acidity, from a starting mixture in 1.0 mol·L^{-1} HNO_3 solution up to an initial pH value of about 10.0. A small amount of ZrO_2 (few wt.%, space group $P2_1/c$) was quantified only for the samples prepared with pH_{ini} = 2.0 and 3.1 (syntheses (3) and (4)). Nevertheless, for higher pH values (syntheses (11) and (12)), the precipitation of an unidentified phase was also evidenced. Contrary to the experiments performed by Valero [39], the formation of $ZrSiO_4$ was observed for an initial pH close to neutrality. However, the prepared silicates exhibited a lower crystallinity than those obtained from higher or lower pH values. Comparing our results with those obtained by Valero, it is likely that nanoscale zircon was obtained in his study rather than an amorphous phase when pH values close to neutrality.

Unit cell parameters were determined by Rietveld refinements of PXRD patterns for all the $ZrSiO_4$ samples prepared between 1.0 mol·L^{-1} HNO_3 and pH_{ini} = 9.0. The obtained values did not allow observing any significant variation of the unit cell parameters with respect to the initial pH of the reactive media. Indeed, the unit cell volume reached a maximum value of 262.7(7) Å^3 (a = 6.628(5) Å and c = 5.980(6) Å) for pH_{ini} = 3.1 and a minimum value of 261.1(7) Å^3 (a = 6.612(5) Å and c = 5.973(6) Å) for 1.0 mol·L^{-1} HNO_3 (**Table SI 2**). No real trend was observed between these two extrema. Such unit cell volumes were found to be slightly bigger than the reference value obtained on sample prepared by dry chemistry route at high temperature (i.e. 260.8 Å^3 (a = 6.604 Å and c = 5.979 Å) [43]. According to recent results published on zircon-based compounds, this difference could be due to the insertion of molecular water or hydroxide groups in the zircon structure [11], [12], [56]. It may be correlated to non-ideal crystallization in the soft hydrothermal conditions considered.

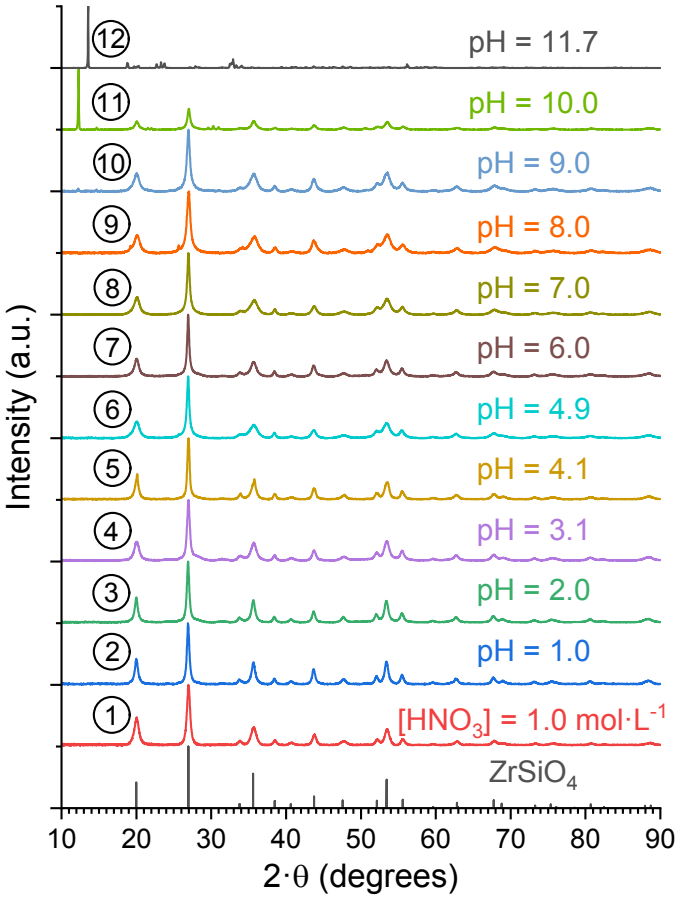

Figure 2. PXRD patterns obtained for $ZrSiO_4$ samples prepared under hydrothermal conditions (20 days, T = 250°C) starting with zirconium and silicate concentrations of 0.2 mol·L^{-1} and for various initial pH values: 1.0 mol.L^{-1} HNO_3 (1), pH = 1.0 (2), pH = 2.0 (3), pH = 3.1 (4), pH = 4.1 (5), pH = 4.9 (6), pH = 6.0 (7), pH = 7.0 (8), pH = 8.0 (9), pH = 9.0 (10), pH = 10.0 (11) and pH = 11.7 (12).

3.1.2. Effect of the hydrothermal treatment duration

In order to observe the impact of the hydrothermal treatment duration on the formation of $ZrSiO_4$, several experiments were also performed at 250°C with an initial pH value equal to 1 and a zirconium concentration of 0.2 mol·L^{-1}. Holding times were fixed to 1, 7 and 20 days. From PXRD analyses (**Figure 3**), single phase $ZrSiO_4$ was always formed showing that the duration of the hydrothermal treatment did not affect the stability of the obtained phase. However, the longer the hydrothermal treatment duration, the better the crystallinity of the final product. This later point supports the data reported in the literature from which the kinetics of crystallization of $ZrSiO_4$ appears to be slower compared to that of $HfSiO_4$ or $ThSiO_4$ [11], [12].

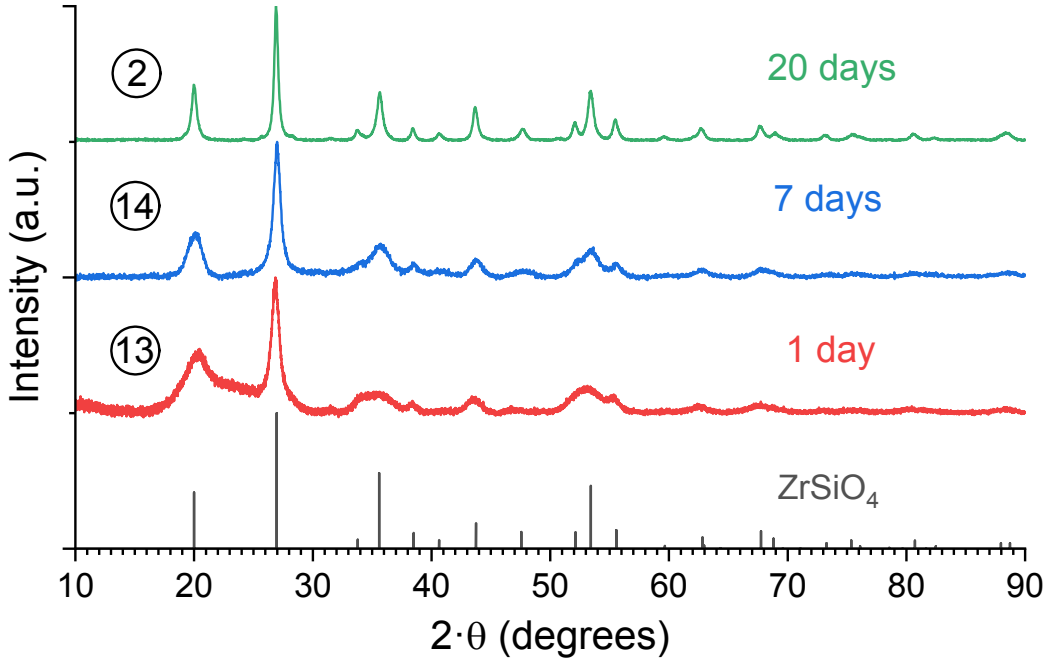

Figure 3. PXRD patterns obtained for $ZrSiO_4$ samples prepared under hydrothermal conditions (T = 250°C, pH = 1) starting with zirconium and silicate concentrations of 0.2 mol·L^{-1} and for holding time of 1 day (13), 7 days (14) and 20 days (2).

Moreover, based on Rietveld refinements (**Figure 4**), extension of the duration of the hydrothermal treatment led to a small, but noticeable, change of the unit cell volume and crystallite size. Indeed, the unit cell volume and the crystallite size reached V = 267(2) Å^3 (a = 6.69(2) Å and c = 5.97(12) Å) and 7 ± 2 nm, respectively, after 1 day compared to V = 262.0(3) Å^3 (a = 6.620(3) Å and c = 5.978(10) Å) and 10 ± 2 nm after 7 days and V = 262.6(2) Å^3 (a = 6.627(1) Å and c = 5.979(3) Å) and 24 ± 2 nm after 7 days. The initial very strong unit cell volume decrease could be explained by the poor crystallization state of the sample obtained after 1 day leading to strong distortion of the zircon lattice. Subsequently, particle size increased, and crystallization state improved with increasing hydrothermal treatment time, due to the Ostwald ripening process.

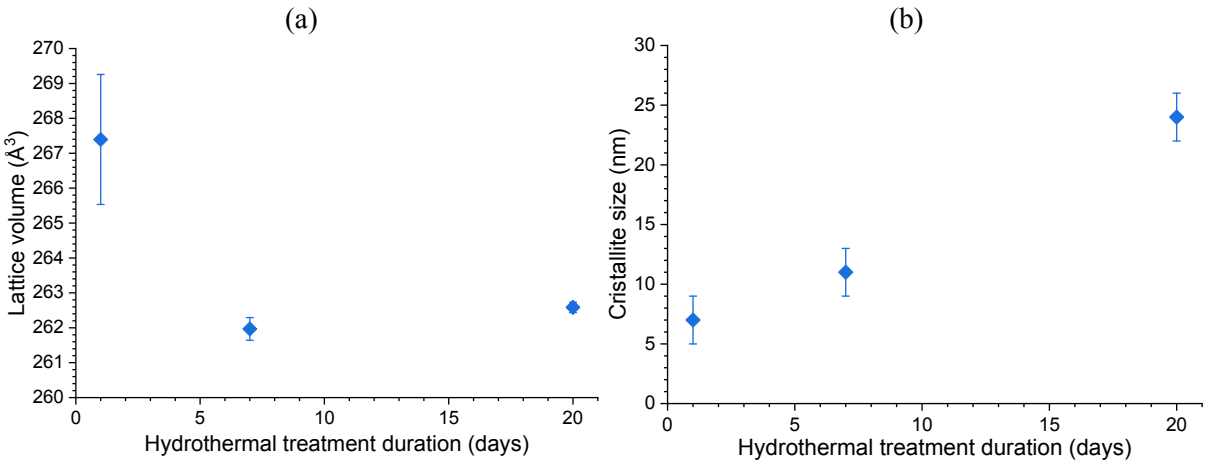

Figure 4. Unit cell volume (a) and average crystallite size (b) determined by Rietveld refinement for $ZrSiO_4$ samples prepared under hydrothermal conditions (T = 250°C) starting with zirconium and silicate concentrations of 0.2 mol·L^{-1} and at pH_{ini} = 1 with hydrothermal treatment duration of 1 day (13), 7 days (14) and 20 days (2).

3.1.3. Effect of the starting zirconium and silicate concentrations

Since the reagent concentrations were crucial parameters for the synthesis of several zircon-group compounds, it was also suspected that the concentrations of zirconium and silicate in the starting mixture affected the formation of $ZrSiO_4$ by varying the saturation index of the solution with respect to zircon. With this objective, several syntheses were performed under hydrothermal conditions with various starting zirconium and silicate concentrations. The impact of the zirconium and silicate concentrations was followed between 0.05 mol·L^{-1} and 1.0 mol·L^{-1}, keeping constant the Si/Zr molar ratio to 1.05, the initial pH value to 1, and the conditions of the hydrothermal treatment (T = 250 °C, 7 days). From the results summarized in **Figure 5**, pure $ZrSiO_4$ was obtained for $C_{Zr} \geq 0.2$ mol·L^{-1} whereas the formation of ZrO_2 was observed as a byproduct for lower concentration such as C_{Zr} = 0.05 mol·L^{-1}. From these observations, one can conclude that silicate concentration in solution was not sufficient to fully counterbalance the hydrolysis of zirconium in the less concentrated media. Therefore, the formation of $ZrSiO_4$ was favored for $C_{Zr} \geq 0.2$ mol·L^{-1}. Moreover, the starting concentration did not seem to really affect the crystallization state of the final sample (**Figure 6**). Regardless the concentration used, the crystallite size obtained was close to 10 nm under the synthesis conditions considered (T = 250°C, 7 days). This was explained by a fast kinetics of zircon nucleation and its very low solubility, which did not promote growth phenomena. Moreover, the very small crystallite sizes measured made it difficult to assess variations. Simultaneously,

the unit cell volume had only a very limited variation and only slightly increased for higher starting concentrations in the reactive medium. Indeed, it varied from $V = 261.9(1)$ Å^3 (a = 6.607(1) Å and c = 5.983(2) Å) for starting concentrations of 0.05 mol·L^{-1} to $V = 262.7(2)$ Å^3 (a = 6.628(2) Å and c = 5.979(8) Å) for starting concentrations of 1.0 mol·L^{-1}. This result might be explained by a higher amount of water/hydroxide groups inserted in the zircon phase for the syntheses performed for high zirconium and silicate starting concentrations.

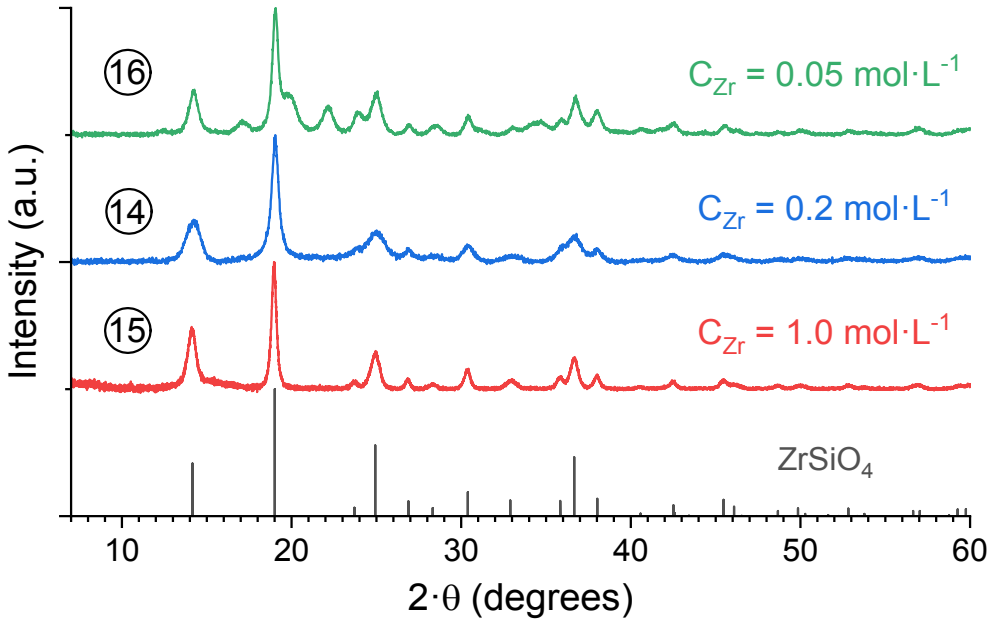

Figure 5. PXRD patterns obtained for $ZrSiO_4$ samples prepared under hydrothermal conditions (T = 250°C, 7 days) at pH = 1.0 starting with zirconium and silicate concentrations of 1.0 mol·L^{-1} (15), 0.2 mol·L^{-1} (14) and 0.05 mol·L^{-1} (16).

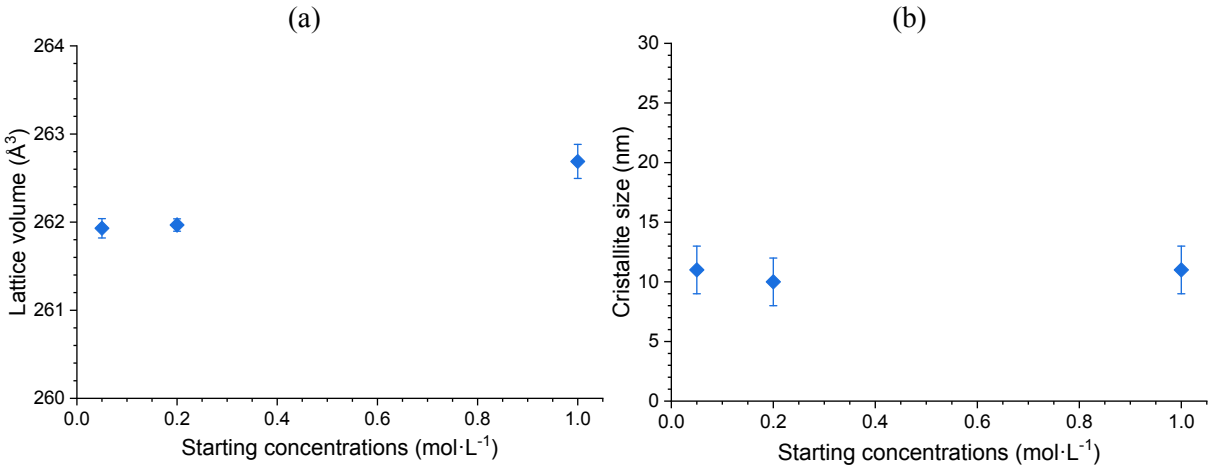

Figure 6. Unit cell volume (a) and average crystallite size (b) determined by Rietveld refinement for $ZrSiO_4$ samples prepared under hydrothermal conditions

(T = 250°C, 7 days, pH =1) starting with zirconium and silicate concentrations of 1.0 mol·L^{-1} (15), 0.2 mol·L^{-1} (14) and 0.05 mol·L^{-1} (16).

3.1.4. Additional characterization of annealed $ZrSiO_4$ sample

Natural zircons are known to be highly hydrated and hydroxylated [44], [57], like several other zircon-group compounds such as coffinite $USiO_4$ [1], [56], [58]. It therefore appeared important to characterize $ZrSiO_4$ samples in the pristine state (washed and dried from hydrothermal synthesis) and after annealing at 1000°C. The characterized $ZrSiO_4$ sample was prepared under hydrothermal conditions at 250°C for 7 days, at pH = 1 and starting from zirconium and silicate concentrations of 0.2 mol·L^{-1}.

First, SEM micrographs were recorded for both $ZrSiO_4$ samples. None of the zircon-type samples exhibited a well-defined morphology. It was composed of very fine nanoparticles gathered in bigger aggregates of few micrometers in size (**Figure SI 1**). These observations were in good agreement with what was reported in the literature for $ZrSiO_4$, although the morphology of this phase appeared to be highly dependent on the precursors used as well as on the initial pH of the starting mixture [43], [59], [60].

TGA analysis (**Figure 7**) revealed that $ZrSiO_4$ was thermally stable up to 1000 °C. The TGA profile obtained was comparable to the data available in the literature for synthetic zircon specimens despite different synthetic conditions [44], [57]. Due to the high total mass loss measured, i.e. 10.5 wt.%, the sample was found to be highly hydrated and hydroxylated. A first mass loss (4.5 wt.%) was observed around 100°C. It was assigned to the elimination of water molecules adsorbed on the surface of the sample. A second mass loss (≈ 4 wt.%) was observed up to about 480 °C. It could be explained by the significant release of the "structural" water confined into the [001] channel, more strongly interacting with the structure of the sample, as suggested by Strzelecki *et al*. [56], [61]. Then, the additional mass loss (≈ 2 wt.%) observed up to 1000 °C, may be due to the continuous release of the most strongly bonded water molecules among with the hydroxyl groups. These results agreed well with the results recently obtained by Guo *et al*. [62] for TGA analyzes of synthetic coffinite $USiO_4$ samples and by Estevenon *et al*. [11], [12] for $HfSiO_4$ and $ThSiO_4$ samples. However, it is known that hydration of synthetic or natural $ZrSiO_4$ samples is erratic and almost always higher than for other silicates of the zircon-group [44], [57], [63].

PXRD patterns of pristine and annealed $ZrSiO_4$ sample confirmed the thermal stability up to 1000°C (**Figure 7**). The zircon-type structure (space group $I4_1/amd$) was preserved and

no trace of oxide formation such as ZrO_2 was evidenced. The unit cell volume decreased from $V = 262.0(3)$ Å^3 ($a = 6.620(3)$ Å and $c = 5.978(3)$ Å) to $V = 260.8(1)$ Å^3 ($a = 6.5995(5)$ Å and $c = 5.987(1)$ Å) after the thermal treatment, again evidencing the release of the confined water molecules and hydroxyl groups. It was also noted that the heat treatment allowed the growth of crystallites, from size of 10 ± 1 nm to 28 ± 1 nm.

Pristine and annealed samples were characterized by SEM. However, no characteristic change of morphology was observed (**Figure SI 1**).

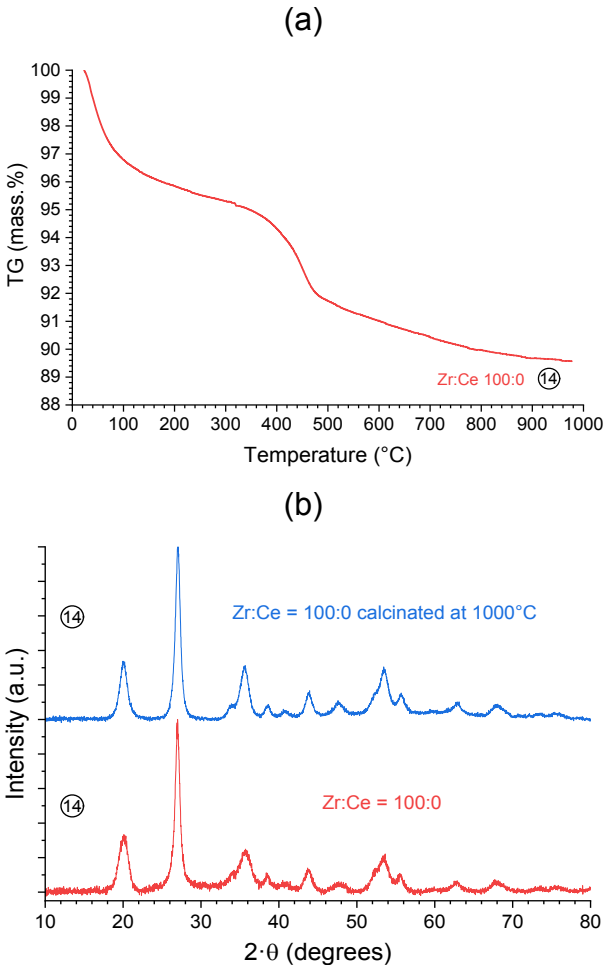

Figure 7. TGA analysis (a) and PXRD patterns (b) recorded for a pristine and annealed (after TGA, 1000°C) $ZrSiO_4$ sample (14) prepared under hydrothermal conditions (T = 250°C, 7 days) at pH = 1.0 starting with zirconium and silicate concentrations of 0.2 mol·L^{-1}.

The analysis by IR and Raman spectroscopies (**Figure 8**) recorded for pristine and annealed $ZrSiO_4$ samples confirmed the previous interpretations. Regarding the Raman spectra, seven vibration bands were evidenced in addition to vibrational bands observed below 300 cm^{-1},

which were attributed to external modes. Then, four vibration bands located near 440 cm^{-1}, 610 cm^{-1}, 970 cm^{-1} and 1000 cm^{-1} belonged to the SiO_4 internal modes ν_2, ν_4, ν_1 and ν_3, respectively. Now focusing on the IR spectra of the pristine zircon sample, the water bending mode band, even with a low intensity, was observed near 1550 cm^{-1}. Moreover, stretching mode of hydroxyl groups, near 2930 cm^{-1}, was clearly visible in the spectrum. Finally, a wide band ranging between 3700 – 3100 cm^{-1} was assigned to the stretching mode band of hydroxide. Thus, the presence of these three vibration bands supported the hydrated and hydroxylated character of $ZrSiO_4$, as often mentioned in the literature for several zircon-type compounds [44], [56], [57], [64]. Especially, annealing step at 1000 °C led to the disappearance of these bands, showing the full dehydration and dehydroxylation of the zircon sample. This result agreed well with that suggested from TGA analysis.

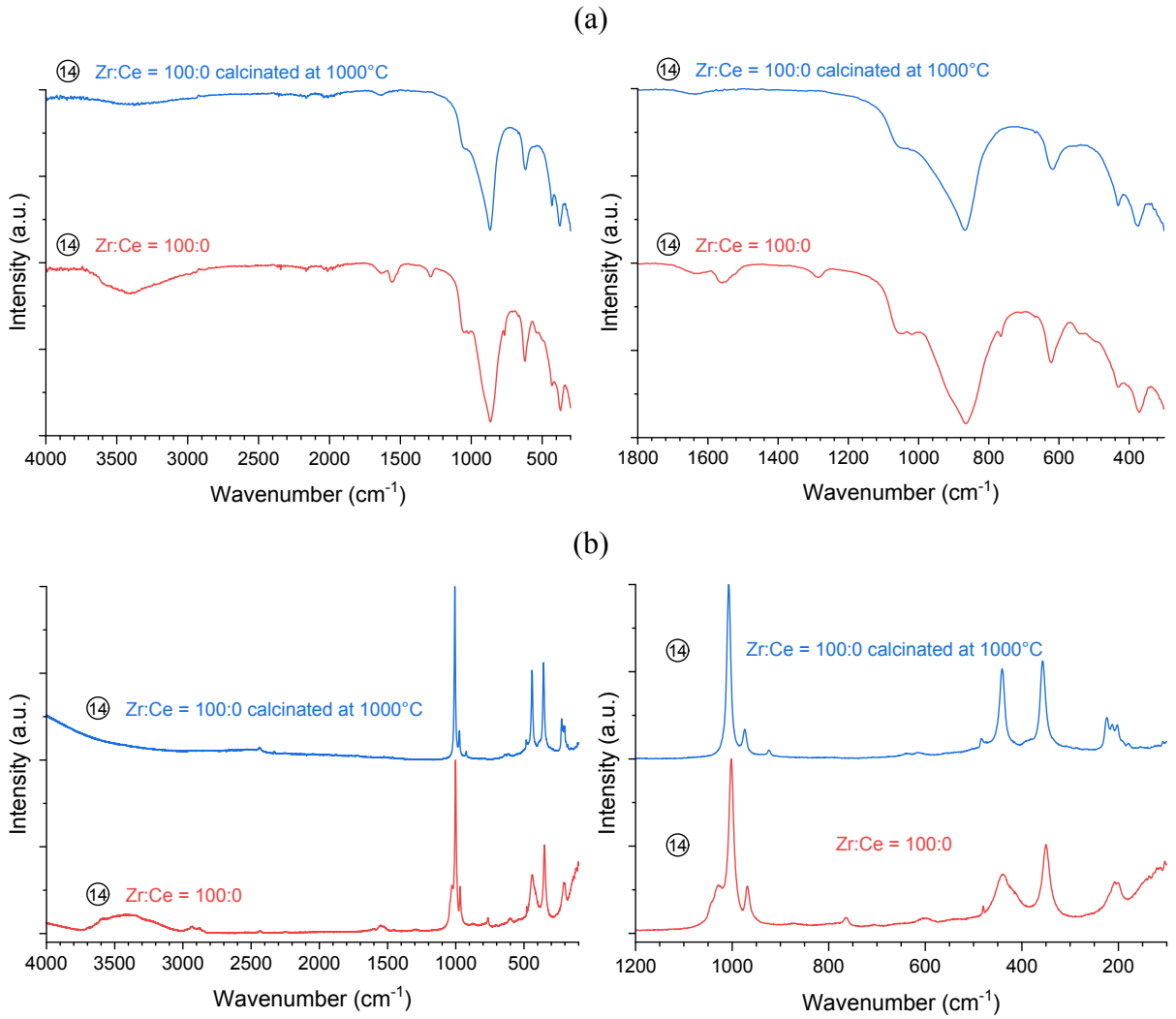

Figure 8. Infrared (a) and Raman (b) spectra recorded in the 4000 – 300 cm^{-1} and 4000 – 100 cm^{-1}, respectively, for pristine (14) and annealed $ZrSiO_4$ sample prepared

under hydrothermal conditions (T = 250°C, 7 days, pH = 1.0) starting with zirconium and silicate concentrations of 0.2 mol·L^{-1}.

3.2 Hydrothermal synthesis of (Zr,Ce)SiO_4 solid solutions

The preparation of solid solutions based on the protocol developed for $CeSiO_4$ was initially suggested. However, this compound was obtained by the slow oxidation of Ce(III) to Ce(IV) in order to avoid hydrolysis of cerium(IV) and hence the formation of the oxide, CeO_2. In contrast to cerium, zirconium the precipitation of cerium silicate appears to be much faster. Under such experimental conditions, it is unlikely that these cations, which exhibit different chemical behaviors, would have led to the formation of a (Zr,Ce)SiO_4 solid solution. For this reason, the experimental optimal conditions considered for the synthesis of (Zr,Ce)SiO_4 solid solutions were first fixed on the basis of those determined for both $ZrSiO_4$ and $CeSiO_4$ end-members. Syntheses were thus performed through hydrothermal treatment at 250°C for 7 days starting with silicate and global Zr + Ce concentrations of 0.2 mol·L^{-1} in nitric acid (pH = 1). Such conditions appeared to be the best compromise to prepare oxide-free and relatively well-crystallized silicates.

3.2.1. PXRD characterization

Results of PXRD analysis showed the formation of (Zr,Ce)SiO_4 solid solutions for Ce incorporation concentrations ranging from 5 mol.% to about 40 mol.% (**Figure 9**). Indeed, PXRD patterns revealed the presence of all XRD lines associated to the tetragonal $I4_1/amd$ zircon-type structure, without any extra peak. Moreover, a progressive shift towards the low angles was observed when increasing the Ce concentration up to 50 mol.%. With sample of Ce 50 mol.% showing secondary phase (CeO_2), XRD results suggested that the solubility limit of Ce in the $ZrSiO_4$ matrix is above 40 mol.%, which is significantly higher than that reported on synthetic specimens prepared by dry chemistry route [24], [25]. Furthermore, a low additional shift was obtained between the samples containing 50 mol.% and 60 mol.% of Ce. It suggested that the limit of cerium incorporation was obtained in that range using this synthesis route. This limit is found to be much higher than those reported in the literature using dry routes of synthesis. Considering that the Ce end-member formation is not possible under such synthesis conditions (see the multiparametric synthesis of $CeSiO_4$ in [33]), this also underlines the important role of zirconium in the co-precipitation of Ce(IV) as a silicate compound.

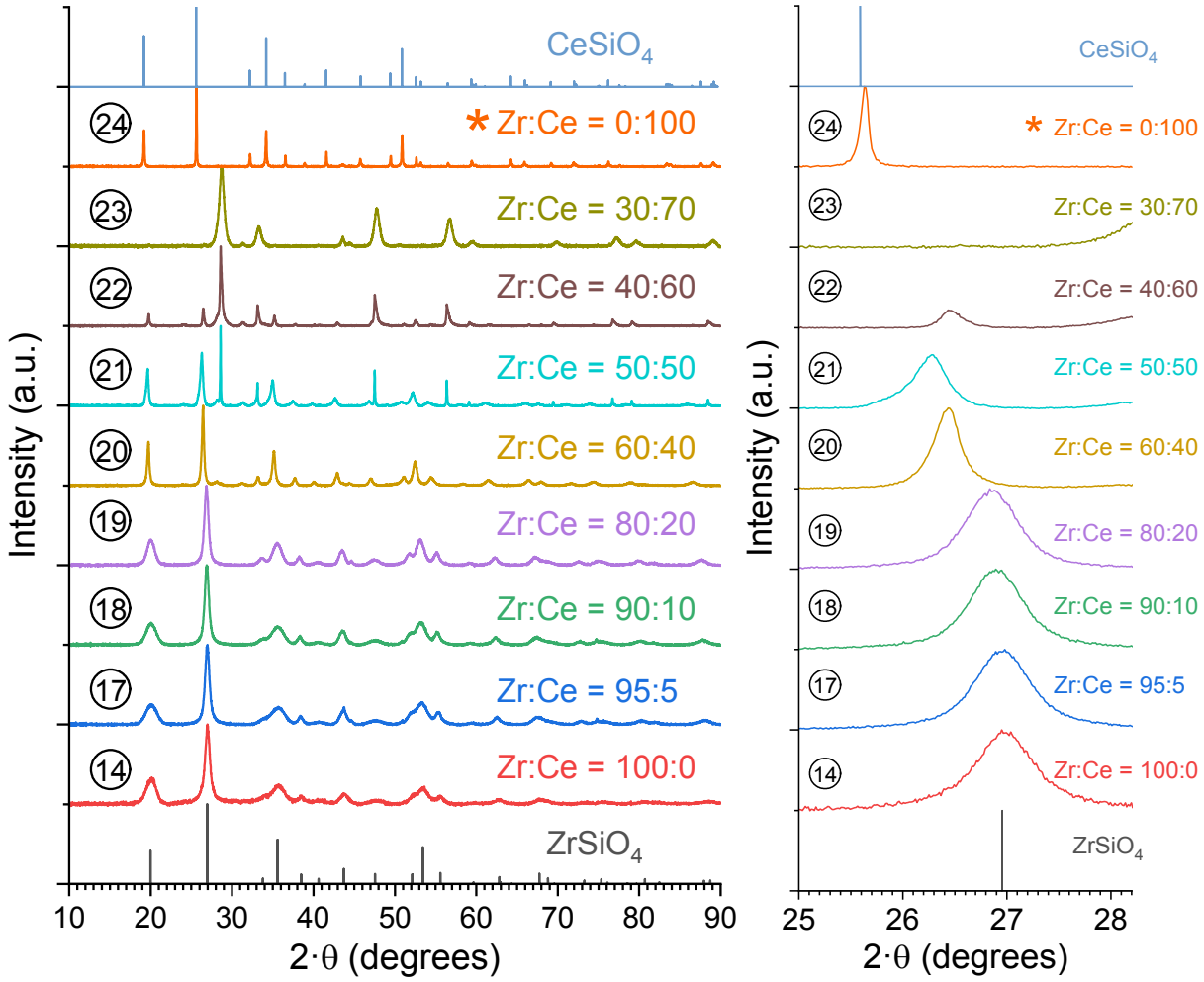

Figure 9. PXRD patterns recorded for pristine (Zr,Ce)SiO_4 solid solutions with various chemical compositions prepared under hydrothermal conditions (T = 250°C, 7 days, pH = 1.0) starting with Zr + Ce and silicate concentrations of 0.2 mol·L^{-1} for Zr:Ce = 100:0 (14), 95:5 (17), 90:10 (18), 80:20 (19), 60:40 (20), 50:50 (21), 40:60 (22) and 30:70 (23). * Reference $CeSiO_4$ sample (T = 150°C, 7 days, pH = 6.5) starting with cerium and silicate concentrations of 0.2 mol·L^{-1} (24).

Since $ZrSiO_4$ dehydration process appeared to be progressive up to 1000°C (**Figure 7a**), samples calcination have been carried out at 800°C and 1000°C in order to prepare water-free (Zr,Ce)SiO_4 samples and to compare the impact of the water loss on the silicate structure. Rietveld refinements were thereafter carried out on all pristine solid solutions (i.e. from 5 to 60 mol.% of Ce) as well as on samples annealed at 800°C and 1000°C to study their thermal stability along with the effect of dehydration on the values of unit cell parameters (**Table 1** and **Figure 10**). Independently of hydration, *a* and *c* unit cell parameters were found to be very close to that expected values if ideal solid solution was assumed. Indeed, the unit cell volume

increased almost linearly as a function of the Ce molar content, following closely Vegard's law, which is in good agreement with the progressive substitution of Zr by Ce within the structure. The small deviation from Vegard's law could be explained by the presence of ZrO_2 or/and CeO_2 in the mixture with silicate, affecting the Ce content of the solid solution, or non-ideal volume of mixing.

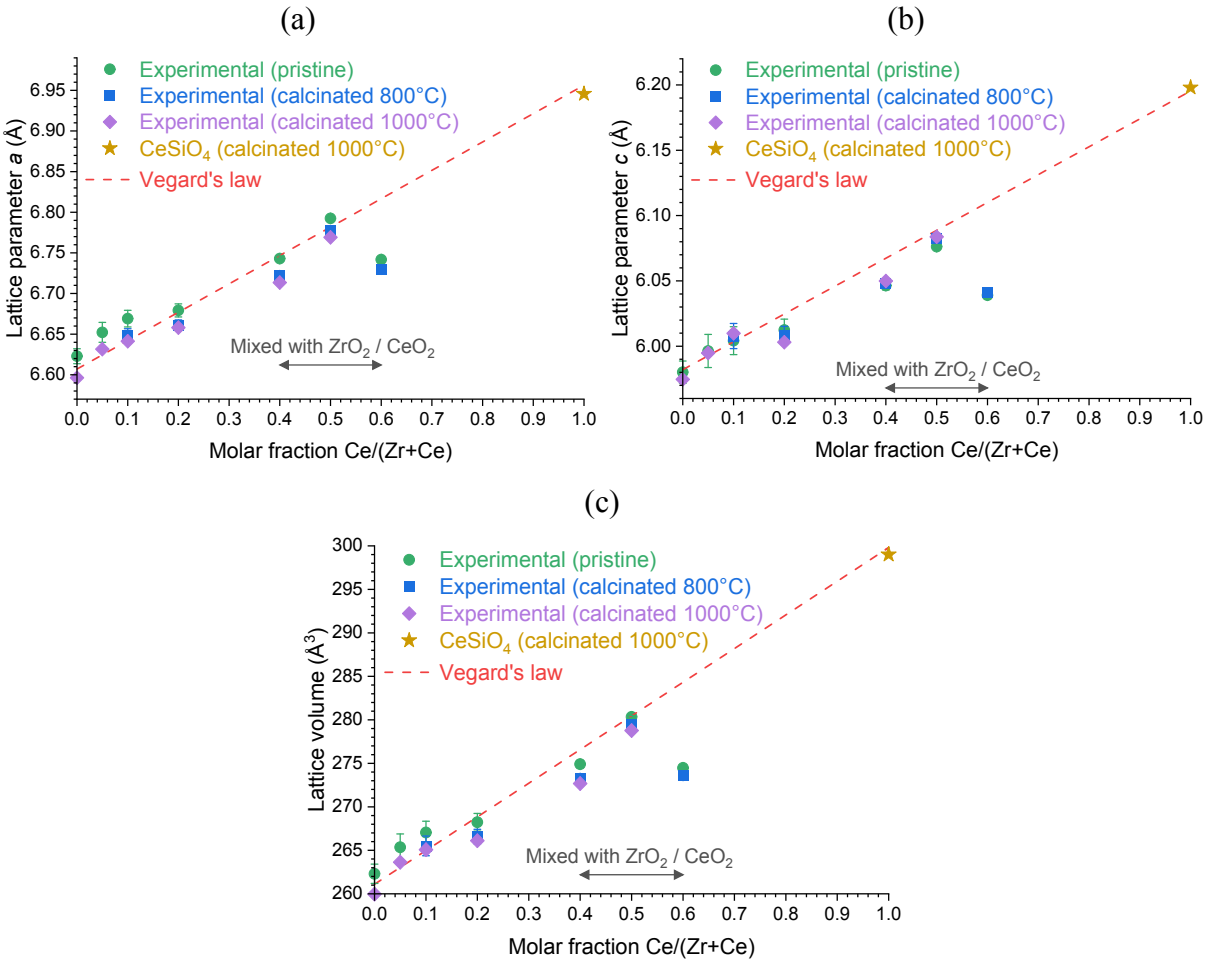

Figure 10. Unit cell parameters *a* (a) and *c* (b) and volume (c) obtained by Rietveld refinements performed from PXRD patterns of pristine (Zr,Ce)SiO_4 solid solutions and annealed samples at 800°C and 1000°C. * Reference $CeSiO_4$ sample was not obtained in the same chemical conditions as the (Zr,Ce)SiO_4 samples.

Regarding to the annealing of the pristine samples, a small decrease of the unit cell volume was first observed. Dehydration led to the contraction of the lattice predominantly in the direction perpendicular to [001] (*i.e. a* and *b* axes). Indeed, water molecules are expected to be located in the channels parallel to [001], which could explain that the *c* axis was not significantly affected [56], [58]. A similar trend has been observed between 800°C and 1000°C

and allows to confirm that the mass loss at high temperature could still be explained by elimination of water molecule. The solid solutions were found to be thermally stable up to at least 1000°C. To improve the detection of secondary phases and the determination of unit cell parameters, the samples annealed at 1000°C were characterized by high resolution PXRD at the MARS beamline of SOLEIL facility (**Figure 11**). The measurement were performed at just below the yttrium K-edge energy (E = 17.0 keV, λ = 0.72959 Å), in order to facilitate the direct comparison with PXRD patterns obtained at the Lab's scale performed at the copper K_α radiation (λ = 1.54184 Å), all of the PXRD patterns have been plotted in scattering vector, according to the Bragg's law, in supporting information (**Figures SI 2** to **SI 7**). Single-phase solid solutions were obtained up to 20 mol.% of Ce. For higher Ce incorporation content, the presence of ZrO_2 as secondary phase was confirmed after annealing at 1000°C (**Figure 11**).

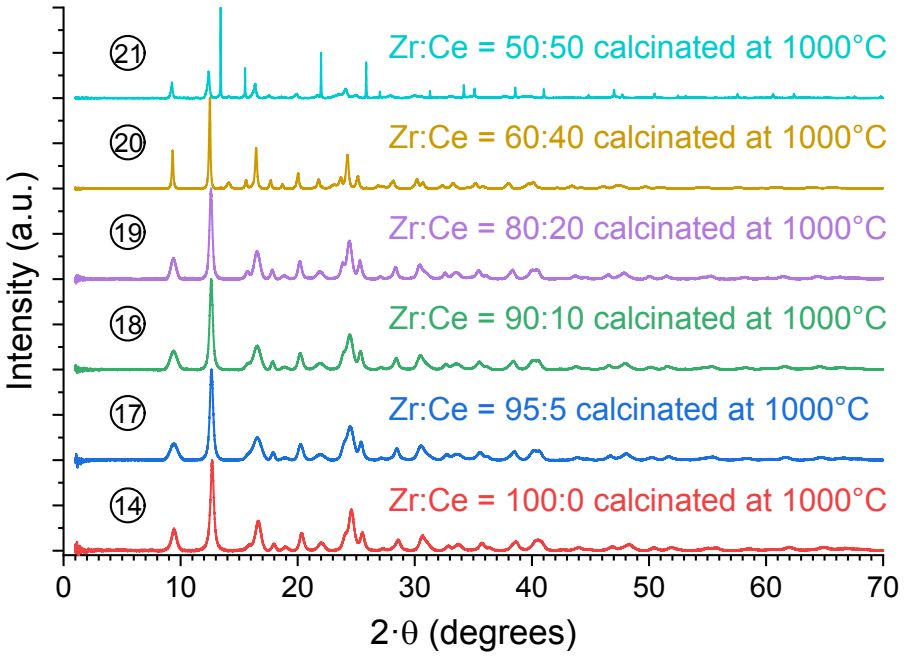

Figure 11. Synchrotron PXRD patterns recorded for $(Zr,Ce)SiO_4$ solid solutions annealed at 1000°C with Zr:Ce = 100:0 (14), Zr:Ce = 95:5 (17), Zr:Ce = 90:10 (18), Zr:Ce = 80:20 (19), Zr:Ce = 60:40 (20) and Zr:Ce = 50:50 (21) prepared under hydrothermal conditions (T = 250°C, 7 days, pH = 1.0) starting with Zr + Ce and silicate concentrations of 0.2 $mol \cdot L^{-1}$.

Table 1 Unit cell parameters and volume obtained by Rietveld refinements performed from PXRD patterns of pristine (Zr,Ce)SiO_4 solid solutions and annealed samples at 800°C or 1000°C.

		Pristine sample			Annealed at 800°C			Annealed at 1000°C		
	$\frac{Ce}{Zr+Ce}$	*a* (Å)	*c* (Å)	*V* (Å)	*a* (Å)	*c* (Å)	*V* (Å)	*a* (Å)	*c* (Å)	*V* (Å)
(14)	0	6.623(9)	5.980(9)	262.3(1)	-	-	-	6.6046(3)	5.9976(4)	261.62(2)
(17)	0.05	6.652(12)	5.996(13)	265.3(15)	-	-	-	6.6335(7)	6.0127(6)	264.58(7)
(18)	0.1	6.669(10)	6.004(11)	267.1(13)	6.648(9)	6.008(10)	265.5(11)	6.6451(4)	6.0239(5)	266.00(3)
(19)	0.2	6.679(8)	6.012(8)	268.2(10)	6.661(7)	6.008(7)	266.6(8)	6.6642(3)	6.0200(4)	267.36(3)
(20)	0.4	6.743(3)	6.046(3)	274.9(4)	6.723(2)	6.048(2)	273.3(3)	6.7188(2)	6.0581(3)	273.48(2)
(21)	0.5	6.792(1)	6.076(1)	280.3(1)	6.778(1)	6.083(2)	279.4(2)	6.7594(5)	6.0985(7)	278.64(4)
(22)	0.6	6.742(2)	6.039(3)	274.4(3)	6.729(2)	6.041(3)	273.6(3)	-	-	-
(24)	1	6.9564(3)	6.1953(4)	299.8(1)	-	-	-	6.9452(2)	6.1978(2)	298.95(2)

The experimental lattice parameters of (Zr,Ce)SiO_4 solid solutions follow fairly closely the variation expected for a Vegard's law between $ZrSiO_4$ and $CeSiO_4$. Since this latter was confirmed as a pure Ce (IV) compound by XANES despite the use of Ce (III) reagents as starting precursors [10], the obtained results suggest the insertion of cerium in the form of Ce (IV) into the $ZrSiO_4$ matrix. Furthermore, this result is supported by the fact that the insertion of Ce^{3+} into $ZrSiO_4$ would be more difficult than that of Ce^{4+} due to the greater difference in ionic radius between Zr^{4+} and Ce^{3+} ions (0.84 Å, 0.97 Å and 1.14 Å for Zr^{4+}, Ce^{4+} and Ce^{3+}, respectively) [29] and to the formation of oxygen vacancies in the zircon-like structure to counterbalance the charge. Therefore, the substitution of Zr^{4+} by Ce^{4+} would induce a 15% increase in ionic size when it would reach 36% when Zr^{4+} is replaced by Ce^{3+}. All these results point to a preferential insertion of Ce^{4+} in $ZrSiO_4$.

3.2.2. Raman and IR characterization

All the prepared samples were characterized by Raman and IR spectroscopies (**Figure 12**). The features associated to the SiO_4 modes were observed on the spectra. The symmetric ν_1 and antisymmetric ν_3 stretching modes were located near to 970 and 1000 cm^{-1} and to 870 and 1070 cm^{-1} by Raman and IR spectroscopies, respectively. Moreover, the ν_2 symmetric bending

mode was observed by both Raman and IR around 440 cm^{-1} while the ν_4 antisymmetric mode was only clearly distinguishable around 620 cm^{-1} in the IR spectra.

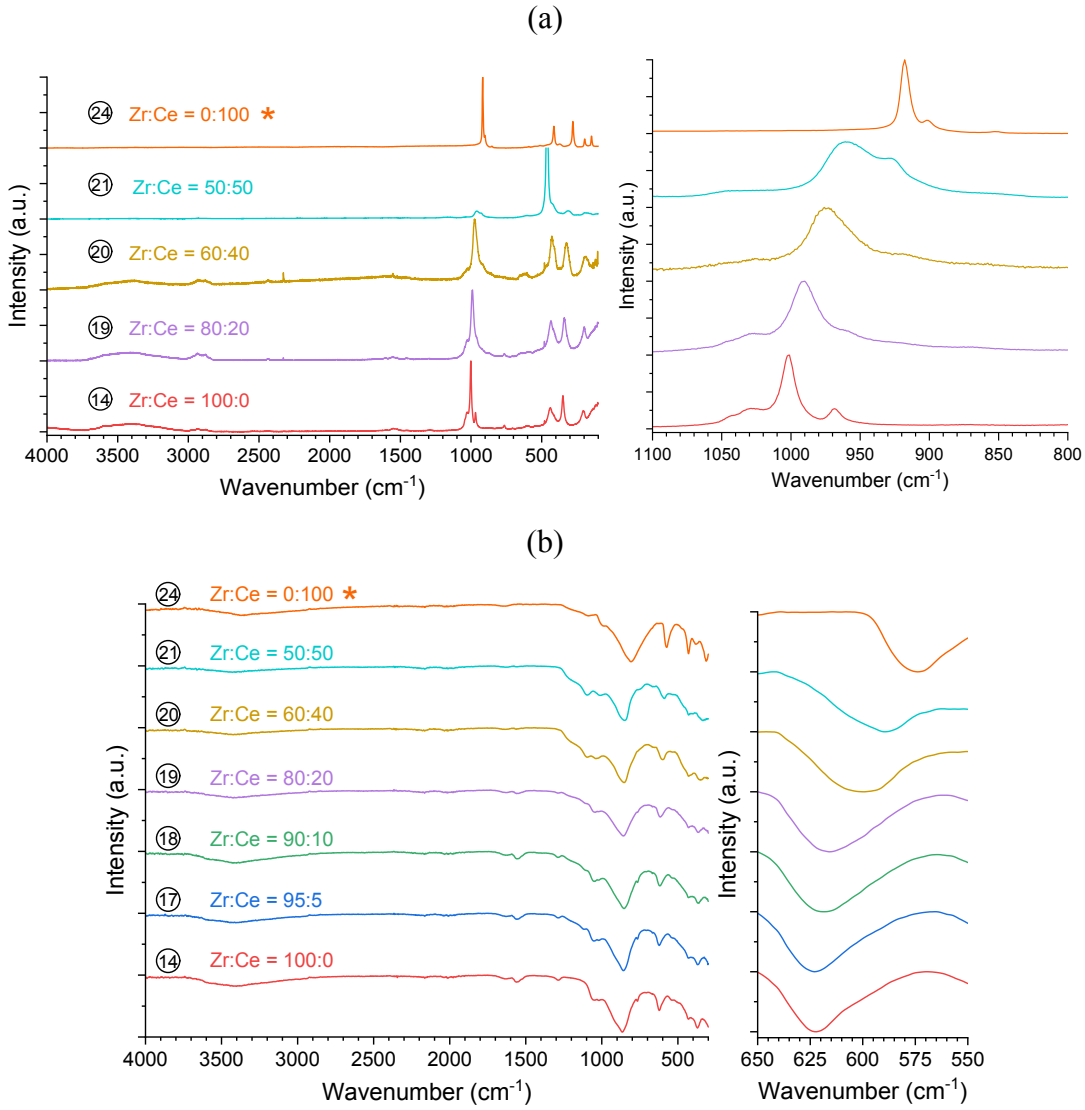

Figure 12. Raman (a) and IR (b) spectra recorded for pristine (Zr,Ce)SiO_4 solid solutions with Zr:Ce = 100:0 (14), Zr:Ce = 95:5 (17), Zr:Ce = 90:10 (18), Zr:Ce = 80:20 (19), Zr:Ce = 60:40 (20), Zr:Ce = 50:50 (21) prepared under hydrothermal conditions (T = 250°C, 7 days, pH = 1.0) starting with Zr + Ce and silicate concentrations of 0.2 mol·L^{-1}. * Reference $CeSiO_4$ sample (T = 150°C, 7 days, pH = 6.5) starting with cerium and silicate concentrations of 0.2 mol·L^{-1} (24).

Additionally, as previously observed for $ZrSiO_4$, Raman and IR spectra suggested the presence of remaining water and/or hydroxyl groups into the pristine samples through the observation of associated weak bands (**Figure 12**). All these bands did not appear anymore after annealing at 1000°C, showing the dehydration/dehydroxylation of the heated samples (**Figure 13**).

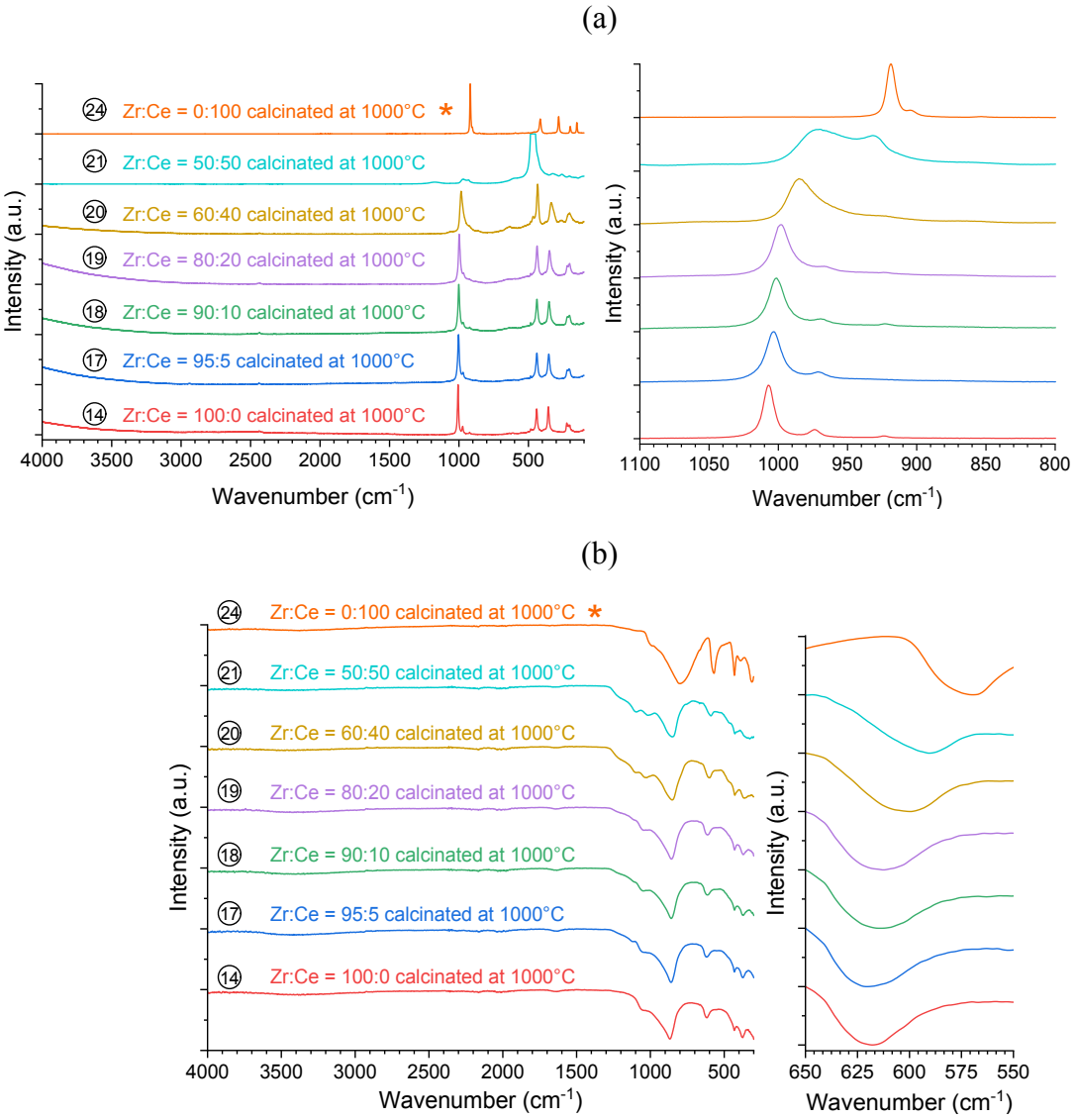

Figure 13. Raman (a) and IR (b) spectra recorded for annealed $(Zr,Ce)SiO_4$ solid solutions with Zr:Ce = 100:0 (14), Zr:Ce = 95:5 (17), Zr:Ce = 90:10 (18), Zr:Ce = 80:20 (19), Zr:Ce = 60:40 (20), Zr:Ce = 50:50 (21) prepared under hydrothermal conditions (T = 250°C, 7 days, pH = 1.0) starting with Zr + Ce and silicate concentrations of 0.2 mol·L^{-1}. * Reference $CeSiO_4$ sample (T = 150°C, 7 days, pH = 6.5) starting with cerium and silicate concentrations of 0.2 mol·L^{-1} (24).

The variations of the vibration bands observed by Raman (ν_2 and ν_3) and IR (ν_1 and ν_4) were plotted for samples annealed at 1000°C versus the chemical composition (**Figure 14** for ν_3 and ν_4, **Figure SI 8** for ν_1 and ν_2). The obtained results are in good agreement with those from PXRD. Indeed, as observed by PXRD, both ν_3 and ν_4 variations followed an almost linear trend which suggested that cerium incorporation increases in $ZrSiO_4$.

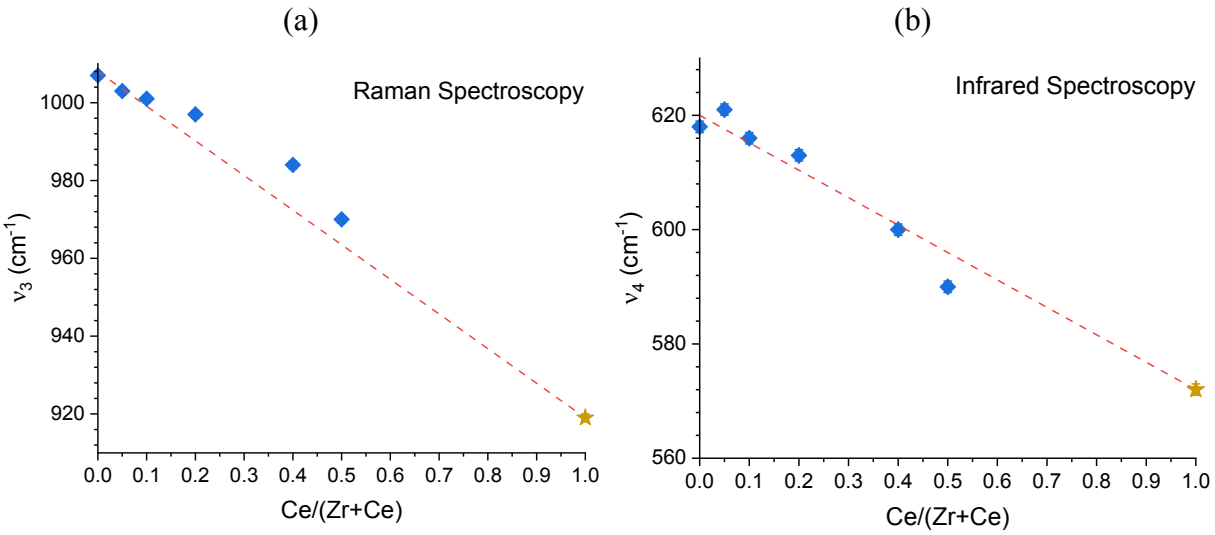

Figure 14. Variation of the ν_3 (a) and ν_4 (b) observed by Raman and IR spectroscopy for $(Zr,Ce)SiO_4$ (annealed samples at 1000°C) versus the expected chemical composition. * Reference $CeSiO_4$ sample wasn't obtained in the same chemical conditions as the $(Zr,Ce)SiO_4$ samples. Errors bars are smaller than the data point size (± 1 cm^{-1}).

3.2.3. Thermogravimetric Analyses

$(Zr,Ce)SiO_4$ samples were characterized by TGA (**Figure 15**). From these results, the weight loss has a negatively correlated dependence on the expected Ce incorporation content. For Ce content below 40 mol.%, TGA curves were close to that recorded for pure $ZrSiO_4$ (**Figure 7a**). The dehydration/dehydroxylation process occurred in three steps for heating temperatures almost independent of the composition. Moreover, the TGA curve of 50 mol.% of Ce agrees well with that of pure $CeSiO_4$. In this case, the dehydration mechanism occurred in only two steps with a weight loss in the same order of magnitude as $CeSiO_4$ (i.e. ≈ 3.5 wt.%) [65]. This is consistent with the fact that pure $ZrSiO_4$ is more prone to hydration and hydroxylation than pure $CeSiO_4$ [56]. Since clear discrimination between water loss and hydroxyl group loss is difficult on the basis of these data alone (in particular due to the losses of water confined in the [001] channels of the silicate phase at high temperatures) [56], we preferred to work with equivalent water content, which includes both water and hydroxide groups, instead of using the more accurate raw formula which could have been written as $(Zr,Ce)(SiO_4)_{1-x}(OH)_{4x}\cdot nH_2O$ (with $x << 1$ for weakly hydroxylated compounds). Indeed, the equivalent water content of pure hydrothermally synthesized $(Zr,Ce)SiO_4$ phases (below 20%) might be quantified from the TGA results leading to chemical formulas: $ZrSiO_4\cdot 1.2H_2O$, $Zr_{0.95}Ce_{0.05}SiO_4\cdot 1.1H_2O$, $Zr_{0.9}Ce_{0.1}SiO_4\cdot 1.2H_2O$ and $Zr_{0.8}Ce_{0.2}SiO_4\cdot 1.0H_2O$ whereas for pure

hydrothermally synthesized $CeSiO_4$, the equivalent water content measured led to the chemical formula $CeSiO_4 \cdot 0.43H_2O$ [56].

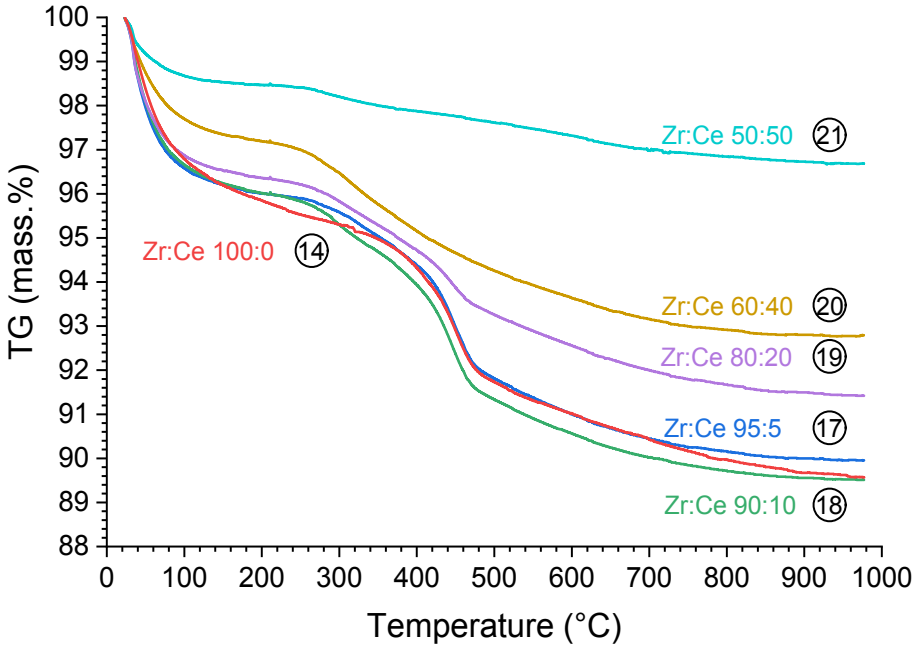

Figure 15. TGA analyses recorded for $(Zr,Ce)SiO_4$ solid solutions with Zr:Ce = 100:0 (14), Zr:Ce = 95:5 (17), Zr:Ce = 90:10 (18), Zr:Ce = 80:20 (19), Zr:Ce = 60:40 (20) and Zr:Ce = 50:50 (21) prepared under hydrothermal conditions (T = 250°C, 7 days, pH = 1.0) starting with Zr + Ce and silicate concentrations of 0.2 $mol \cdot L^{-1}$.

3.2.4. Observations by SEM

SEM micrographs were recorded for several pristine $(Zr,Ce)SiO_4$ samples (**Figure 16**). The prepared samples did not exhibit a well-defined morphology as they were composed of very fine nanoparticles gathered in bigger aggregates of few micrometers in size, as observed for $ZrSiO_4$ (**Figure 16a**). On the contrary, $CeSiO_4$ grains exhibited a well-defined morphology with the formation of square-based bipyramids characteristic of this zircon-type materials [10]. Such differences can result from the distinct conditions of synthesis considered for $ZrSiO_4$ and $(Zr,Ce)SiO_4$, on the one hand, and $CeSiO_4$, on the other hand.

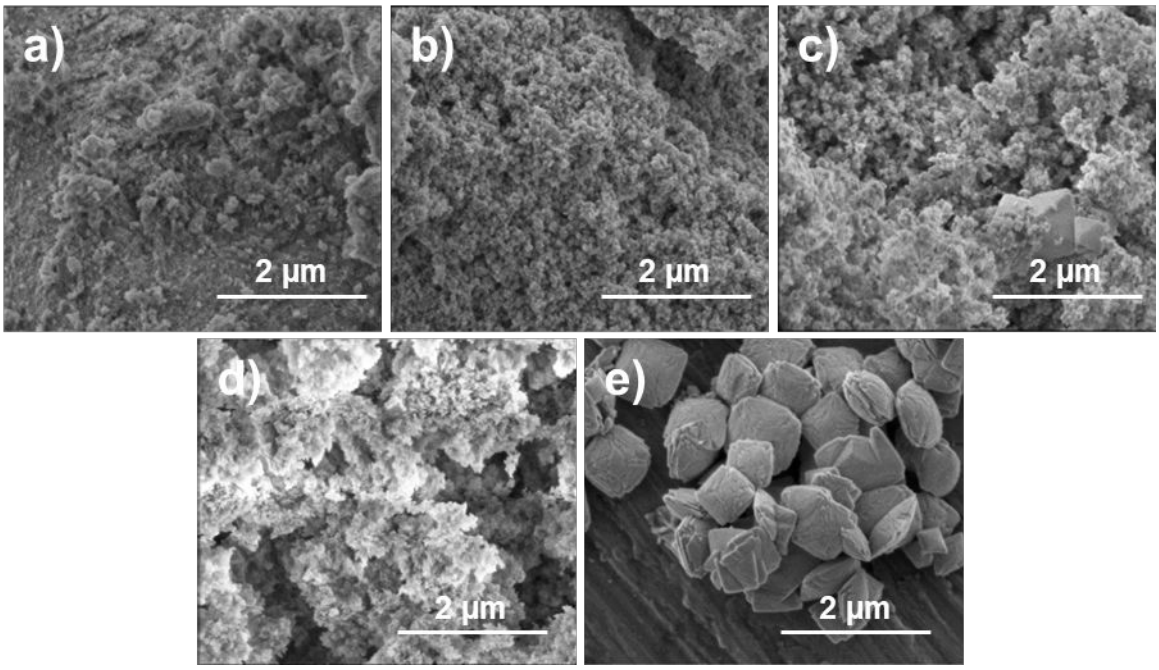

Figure 16. SEM micrographs recorded for $(Zr,Ce)SiO_4$ solid solutions with **a)** Zr:Ce = 100:0 (14), **b)** Zr:Ce = 60:40 (20), **c)** Zr:Ce = 50:50 (21), **d)** Zr:Ce = 30:70 (23) prepared under hydrothermal conditions (T = 250°C, 7 days, pH = 1.0) starting with Zr + Ce and silicate concentrations of 0.2 $mol \cdot L^{-1}$. **e)** Reference $CeSiO_4$ sample (T = 150°C, 7 days, pH = 6.5) starting with cerium and silicate concentrations of 0.2 $mol \cdot L^{-1}$ (24).

4. CONCLUSION

A multiparametric study of $ZrSiO_4$ synthesis under hydrothermal conditions has been performed at 250°C in nitric acid media by varying several experimental parameters, including pH, hydrothermal treatment duration and zirconium and silicate concentrations in the reactive media. The results allowed us to determine an appropriate set of hydrothermal conditions to prepare single phased samples, which are listed below:

- initial pH ranging from $[HNO_3]$ = 1.0 $mol \cdot L^{-1}$ to pH = 9.0;
- the longer is the hydrothermal treatment, the better is the crystallization state; 7 days being a good compromise;
- zirconium and silicate concentration over 0.2 $mol \cdot L^{-1}$ with a Si/Zr molar ratio of 1.05.

$ZrSiO_4$ samples obtained with a pH close to the neutrality appeared to be less crystallized than those obtained for higher or lower pH values more likely explained by the formation of nanoscale zircon than an amorphous phase formation. The $ZrSiO_4$ sample prepared in the

optimal conditions did not exhibit a well-defined morphology. It was found to be highly hydrated and hydroxylated with a thermal stability up to 1000°C.

On the basis of the optimal experimental conditions previously determined for $ZrSiO_4$, the formation of $(Zr,Ce)SiO_4$ solid solution by hydrothermal treatment was studied. Thus, the synthesis tests were performed with a cation (Zr + Ce) concentration of 0.2 $mol \cdot L^{-1}$ in a nitric acid media, a pH value equal to 1 and a hydrothermal treatment at 250°C for 7 days. In these conditions, well crystallized and oxide-free solid solutions were obtained up to 20 mol.% of Ce incorporation. Moreover, the experiment performed to reach higher incorporation contents led to mixture with ZrO_2 and/or CeO_2 phases but suggested that the solubility limit of Ce in the $ZrSiO_4$ matrix reached almost 40 mol.%, well above the values usually obtained for $(Zr,Ce)SiO_4$ solid solutions [24], [25]. Solid solutions with higher cerium incorporation rate might be obtained by using chemical route closer to that allowing the formation of the pure $CeSiO_4$ end-member [9], [33]. However, due to the importance of the cerium redox variation in the $CeSiO_4$ synthesis process, the Ce substitution by a pure tetravalent reactant, like Zr(IV), could be difficult.

As for $ZrSiO_4$, the $(Zr,Ce)SiO_4$ samples did not exhibit a well-defined morphology, and were found to be highly hydrated (raw formula of pure $(Zr,Ce)SiO_4$ phases: $ZrSiO_4 \cdot 1.2H_2O$, $Zr_{0.95}Ce_{0.05}SiO_4 \cdot 1.1H_2O$, $Zr_{0.9}Ce_{0.1}SiO_4 \cdot 1.2H_2O$, $Zr_{0.8}Ce_{0.2}SiO_4 \cdot 1.0H_2O$), with dehydrated phases thermally stable up to 1000°C regardless of the Ce content.

These results are particularly interesting in the context of studies that could be carried out on $(Zr,An)SiO_4$ solid solutions that formed under accidental conditions and could allow the evaluation of the physical properties of these solid solutions. In this perspective, a complementary calorimetry study is now under progress to learn more about the thermodynamic properties of $(Zr,Ce)SiO_4$ solid solutions. It would be a first step in the perspective of studying $(Zr,U)SiO_4$ and $(Zr,Pu)SiO_4$ solid solutions.

REFERENCES

[1] R. J. Finch and J. M. Hanchar, "Structure and chemistry of Zircon and Zircon-Group minerals," *Rev. Mineral. Geochemistry*, vol. 53, no. 1, pp. 1–25, 2003, doi: 1529-6466/03/0053-0001$05.00.

[2] K. Von Chrustschoff, "On the artificial production of zircon in the wet way," *Jahrb. für Mineral.*, vol. 2, 1892.

[3] B. E. B. Anderson, B. E. Burakov, and E. M. Pazukhin, "High-Uranium Zircon from " Chernobyl Lavas "," *Radiochim. Acta*, vol. 151, pp. 149–151, 1993, doi: 0033-8230/93 $ 3.00+0.00.

[4] T. Geisler, B. E. Burakov, V. Zirlin, L. Nikolaeva, and P. Pöml, "A Raman spectroscopic study of high-uranium zircon from the Chernobyl ' lava ,'" *Eur. J. Mineral.*, vol. 17, pp. 883–894, 2015, doi: 10.1127/0935-1221/2005/0017-0883.

[5] H. Ding *et al.*, "Chemical characterisation of degraded nuclear fuel analogues simulating the Fukushima Daiichi nuclear accident," *npj Mater. Degrad.*, vol. 6, no. 10, pp. 1–13, 2022, doi: 10.1038/s41529-022-00219-3.

[6] R. C. Ewing, "Nuclear waste forms for actinides," *Proc. Natl. Acad. Sci.*, vol. 96, pp. 3432–3439, 1999.

[7] W. J. Weber, R. C. Ewing, and W. Lutze, "Performance assessment of zircon as a waste form for excess weapons plutonium under deep borehole burial conditions," *Mater. Res. Soc. Symp. Proc.*, vol. 412, pp. 25–32, 1996.

[8] R. C. Ewing and W. Lutze, "Zircon: A host-phase for the disposal of weapons plutonium," *J. Mater. Res.*, vol. 10, no. 2, pp. 243–246, 1995, doi: 10.1557/JMR.1995.0243.

[9] H. R. Hoekstra and L. H. Fuchs, "Synthesis of coffinite - USiO4," *Science (80-.).*, vol. 123, p. 105, 1956.

[10] P. Estevenon *et al.*, "Formation of CeSiO4 from cerium(III) silicate precursors," *Dalt. Trans.*, vol. 48, no. 28, pp. 10455–10463, 2019, doi: 10.1039/c9dt01990a.

[11] P. Estevenon *et al.*, "Soft Hydrothermal Synthesis of Hafnon, HfSiO4," *Cryst. Growth Des.*, vol. 20, pp. 1820–1828, 2020, doi: 10.1021/acs.cgd.9b01546.

[12] P. Estevenon *et al.*, "Multiparametric Study of the Synthesis of ThSiO4 under Hydrothermal Conditions," *Inorg. Chem.*, vol. 57, pp. 9393–9402, 2018, doi: 10.1021/acs.inorgchem.8b01390.

[13] P. Estevenon *et al.*, "The formation of PuSiO4 under hydrothermal conditions," *Dalt. Trans.*, vol. 49, no. 19, pp. 6434–6445, 2020, doi: 10.1039/d0dt01183e.

[14] C. Keller, "Untersuchungen über die Germanate und Silikate des Typs ABO4 der vierwertigen Elemente Thorium bis Americium," *Nukleonik*, vol. 5, no. 2, pp. 41–48, 1963.

[15] S. S. Ramakrishnan, K. V. G. K. Gokhale, and E. C. Subbarao, "Solid solubility in the system zircon - hafnon," *Mater. Res. Bull.*, vol. 4, pp. 323–327, 1969, doi:

10.1016/0025-5408(69)90036-1.

[16] P. W. . Hoskin and K. A. Rodgers, “Raman spectral shift in the isomorphous series (Zr1-xHfx)SiO4,” *Eur. J. Solid State Inorg. Chem.*, vol. 33, pp. 1111–1121, 1996.

[17] A. M. Grüneberger, C. Schmidt, S. Jahn, D. Rhede, A. Loges, and M. Wilke, “Interpretation of Raman spectra of the zircon–hafnon solid solution,” *Eur. J. Mineral.*, vol. 28, no. 4, pp. 721–733, 2016, doi: 10.1127/ejm/2016/0028-2551.

[18] A. Cota, B. P. Burton, P. Chaín, E. Pavón, and M. D. Alba, “Solution Properties of the System ZrSiO4-HfSiO4: Computational and Experimental Study,” *J. Phys. Chem. C*, vol. 117, pp. 10013–10019, 2013, doi: 10.1021/jp401539g.

[19] D. T. Costin *et al.*, “How to explain the difficulties in the coffinite synthesis from the study of uranothorite?,” *Inorg. Chem.*, vol. 50, pp. 11117–11126, 2011, doi: 10.1021/ic2016758.

[20] D. T. Costin *et al.*, “Preparation and characterization of synthetic Th0.5U0.5SiO4 uranothorite,” *Prog. Nucl. Energy*, vol. 57, pp. 155–160, 2012, doi: 10.1016/j.pnucene.2011.10.004.

[21] N. Clavier, S. Szenknect, D. T. Costin, A. Mesbah, C. Poinssot, and N. Dacheux, “From thorite to coffinite: A spectroscopic study of Th1−xUxSiO4 solid solutions,” *Spectrochim. Acta Part A Mol. Biomol. Spectrosc.*, vol. 118, pp. 302–307, 2014, doi: 10.1016/j.saa.2013.08.093.

[22] X. Guo *et al.*, “Energetics of a Uranothorite (Th1−xUxSiO4) Solid Solution,” *Chem. Mater.*, vol. 28, pp. 7117–7124, 2016, doi: 10.1021/acs.chemmater.6b03346.

[23] J. Marcial *et al.*, “Thermodynamic non-ideality and disorder heterogeneity in actinide silicate solid solutions,” *npj Mater. Degrad.*, vol. 5, no. 34, pp. 1–14, 2021, doi: 10.1038/s41529-021-00179-0.

[24] S. V Ushakov, W. Gong, M. M. Yagovkina, K. B. Helean, W. Lutze, and R. C. Ewing, “Solid solutions of Ce, U and Th in zircon,” *Ceram. Trans.*, vol. 93, pp. 357–363, 1999.

[25] S. V. Ushakov *et al.*, “Synthesis of Ce-doped zircon by a sol-gel process,” *Mater. Res. Soc. Symp. Proc.*, vol. 506, pp. 281–288, 1998.

[26] B. E. Burakov *et al.*, “Synthesis of Zircon for immobilization of actinides,” *Mater. Res. Soc. Symp. Proc.*, vol. 412, pp. 33–39, 1996.

[27] E. D. A. Ferriss, R. C. Ewing, and U. Becker, “Simulation of thermodynamic mixing properties of actinide-containing zircon solid solutions,” *Am. Mineral.*, vol. 95, pp. 229–241, 2010, doi: 10.2138/am.2010.3318.

[28] B. E. Burakov, M. V. Zamoryanskaya, V. M. Garbuzov, V. A. Zirlin, and J. M. Hanchar, “Synthesis and investigation of Pu-doped single crystal zircon, (Zr, Pu)SiO4,” *Radiochim. Acta*, vol. 90, pp. 95–97, 2002, doi: 10.1524/ract.2002.90.2_2002.95.

[29] R. D. Shannon, “Revised Effective Ionic Radii and Systematic Study of Inter Atomic Distances in Halides and Chalcogenides in Halides and Chaleogenides,” *Acta*

Crystallogr., vol. 32, pp. 751–767, 1976, doi: 10.1107/s0567739476001551.

[30] J. M. Hanchar, B. E. Burakov, M. V. Zamoryanskaya, V. M. Garbuzov, A. A. Kitsay, and V. A. Zirlin, "Investigation of Pu Incorporation into Zircon Single Crystal," *Mater. Res. Soc. Symp. Proc.*, vol. 824, p. CC4.2.1-CC4.2.5, 2004, doi: 10.1557/PROC-824-CC4.2.

[31] F. A. Mumpton and R. Roy, "Hydrothermal stability studies of the zircon-thorite group," *Geochim. Cosmochim. Acta*, vol. 21, pp. 217–238, 1961, doi: 10.1016/s0016-7037(61)80056-2.

[32] D. A. Zamyatin, Y. V. Shchapova, S. L. Votyakov, N. N. Eremin, and V. S. Urusov, "Structure and thermodynamic properties of zircon-coffinite solid solutions according to the semiempirical atomistic simulation data," *Glas. Phys. Chem.*, vol. 39, no. 2, pp. 182–192, 2013, doi: 10.1134/S108765961302017X.

[33] V. Grover and A. K. Tyagi, "Preparation and bulk thermal expansion studies in M1-xCe xSiO4 (M = Th, Zr) system, and stabilization of tetragonal ThSiO4," *J. Alloys Compd.*, vol. 390, pp. 112–114, 2005, doi: 10.1016/j.jallcom.2004.05.091.

[34] P. Estevenon *et al.*, "Impact of Carbonate Ions on the Synthesis of ThSiO4 under Hydrothermal Conditions," *Inorg. Chem.*, vol. 57, pp. 12398–12408, 2018, doi: 10.1021/acs.inorgchem.8b02146.

[35] P. Estevenon *et al.*, "Preparation of CeSiO4 from aqueous precursors under soft hydrothermal conditions," *Dalt. Trans.*, vol. 48, no. 22, pp. 7551–7559, 2019, doi: 10.1039/c9dt01258c.

[36] H. S. Kim, C. Y. Joung, B. H. Lee, J. Y. Oh, Y. H. Koo, and P. Heimgartner, "Applicability of CeO2 as a surrogate for PuO2 in a MOX fuel development," *J. Nucl. Mater.*, vol. 378, pp. 98–104, 2008, doi: 10.1016/j.jnucmat.2008.05.003.

[37] B. A. Bilal and E. Müller, "Thermodynamic Study of Ce4+/Ce3+ Redox Reaction in Aqueous Solutions at Elevated Temperatures: 1. Reduction Potential and Hydrolysis Equilibria of Ce4+ in HC104Solutions," *Zeitschrift fur Naturforsch. - Sect. A J. Phys. Sci.*, vol. 47, pp. 974–984, 1992, doi: 10.1515/zna-1992-0908.

[38] R. Guillaumont *et al.*, *Update on the Chemical Thermodynamics of Uranium, Neptunium, Plutonium, Americium and Technetium*. 2003.

[39] R. Valero, "Mécanismes de la synthèse hydrothermale du zircon," Université de Haute Alsace: Mulhouse, France, 1997.

[40] C. Frontera and J. Rodriguez-Carvajal, "FullProf as a new tool for flipping ratio analysis," *Phys. B*, vol. 335, pp. 219–222, 2003, doi: 10.1016/S0921-4526(03)00241-2.

[41] M. Jizzini, E. Brackx, P. Piluso, D. Menut, and R. Guinebretière, "Cationic local composition fluctuations in rapidly cooled nuclear fuel melts," *Nucl. Mater. Energy*, vol. 31, no. 2022, p. 101183, 2022, doi: 10.1016/j.nme.2022.101183.

[42] A. A. Coelho, "computer programs TOPAS and TOPAS-Academic : an optimization program integrating computer algebra and crystallographic objects written in C ++," *J. Appl. Crystallogr.*, vol. 51, pp. 210–218, 2018, doi: 10.1107/S1600576718000183.

[43] R. Caruba, A. Baumer, and G. Turco, “Nouvelles synthéses hydrothermales du zircon: substitutions isomorphiques; relation morphologie-milieu de croissance,” *Geochim. Cosmochim. Acta*, vol. 39, pp. 11–26, 1975, doi: 10.1016/0016-7037(75)90181-7.

[44] R. Caruba, A. Baumer, M. Ganteaume, and P. Iacconi, “An experimental study of hydroxyl groups and water in synthetic and natural zircons: a model of the metamict state.,” *Am. Mineral.*, vol. 70, pp. 1224–1231, 1985, doi: 0003-004X/85/1112-1224$02.00.

[45] C. Frondel and R. L. Collette, “Hydrothermal synthesis of zircon, thorite and huttonite,” *Am. Mineral.*, vol. 42, no. November-December, pp. 759–765, 1957.

[46] R. Valéro, J. L. Paillaud, B. Durand, J. L. Guth, and T. Chopin, “Rietveld refinement of two fluoro-hydroxy-zircons,” *Eur. J. Solid State Inorg. Chem.*, vol. 35, pp. 735–743, 1998, doi: 10.1016/S0992-4361(99)80013-7.

[47] R. Valéro, B. Durand, J. L. Guth, and T. Chopin, “Influence des ions fluorure et de la silice amorphe sur la solubilite des gels de zircone et caracterisation des fluoro-complexes de zirconium en milieu moyennement acide,” *Can. J. Chem.*, vol. 77, pp. 2099–2104, 1999, doi: 10.1139/v99-204.

[48] R. Valéro, B. Durand, J. L. Guth, and T. Chopin, “Hydrothermal synthesis of porous zircon in basic fluorinated medium,” *Microporous Mesoporous Mater.*, vol. 29, pp. 311–318, 1999, doi: 10.1016/S1387-1811(98)00344-8.

[49] R. Valéro, L. Delmotte, J. L. Paillaud, B. Durand, J. L. Guth, and T. Chopin, “A new hydrothermal fluoro-zircon,” *J. Mater. Chem.*, vol. 9, pp. 117–123, 1999, doi: 10.1039/A805924A.

[50] R. Valero, B. Durand, J. L. Guth, and T. Chopin, “Mechanism of Hydrothermal Synthesis of Zircon in a Fluoride Medium,” *J. Sol-Gel Sci. Technol.*, vol. 13, pp. 119–124, 1998, doi: 10.1023/a:1008619809397.

[51] H. Kido and S. Komarneni, “Hydrothermal Processing of Zircon,” *Trans. Mater. Res. Soc. Japan*, pp. 358–369, 1990, doi: 10.1007/978-94-009-0789-8_27.

[52] A. Mosset, P. Baules, P. Lecante, J.-C. Trombe, H. Ahamdane, and F. Bensamka, “A new solution route to silicates Part 4. Submicronic zircon powders.,” *J. Mater. Chem.*, vol. 6, no. 9, pp. 1527–1532, 1996, doi: 10.1039/jm9960601527.

[53] R. Dharmarajan, R. F. Belt, and R. C. Puttbach, “Hydrothermal and flux growth of zircon crystals,” *J. Cryst. Growth*, vol. 13–14, pp. 535–539, 1972, doi: 10.1016/0022-0248(72)90294-1.

[54] S. Komarneni and R. Roy, “Synthesis of zircon,” in *Transactions of the Materials Research Society of Japan*, 1990, pp. 329–339.

[55] R. Uhrin, R. F. Belt, and R. C. Puttbach, “The hydrothermal growth of zircon,” *J. Cryst. Growth*, vol. 21, pp. 65–68, 1974, doi: 10.1016/0022-0248(74)90151-1.

[56] A. C. Strzelecki *et al.*, “The Role of Water and Hydroxyl Groups in the Structures of Stetindite and Coffinite, MSiO4(M = Ce, U),” *Inorg. Chem.*, vol. 60, pp. 718–735, 2021, doi: 10.1021/acs.inorgchem.0c02757.

[57] L. Nasdala, A. Beran, E. Libowitzky, and D. Wolf, “The incorporation of hydroxyl groups and molecular water in natural zircon (ZrSiO4),” *Am. J. Sci.*, vol. 301, pp. 831–857, 2001, doi: 10.2475/ajs.301.10.831.

[58] J. Janeczek and R. C. Ewing, “Coffinitization - A mechanism for the alteration of UO2 under reducing conditions,” *Mater. Res. Soc. Symp. Proc.*, vol. 257, pp. 497–504, 1992.

[59] L. Kljajevic, B. Matovic, S. Nenadovic, Z. Bascarevic, N. Cveticanin, and A. Devecerski, “Fabrication of ZrC/SiC, ZrO2/SiC and ZrO2 powders by carbothermal reduction of ZrSiO4,” *Process. Appl. Ceram.*, vol. 5, pp. 103–112, 2011, doi: 10.2298/pac1102103k.

[60] T. Satish Kumar, R. Raghu, K. Krishna Kumar, S. Shalini, and R. Subramanian, “Optimization of three body abrasive wear behaviour of stir cast A356/ ZrSiO4 metal matrix composite,” *Tribol. Ind.*, vol. 40, no. 4, pp. 633–642, 2018, doi: 10.24874/ti.2018.40.04.10.

[61] A. C. Strzelecki *et al.*, “Crystal Chemistry and Thermodynamics of HREE (Er, Yb) Mixing in a Xenotime Solid Solution,” *ACS Earth Sp. Chem.*, vol. 6, pp. 1375–1389, 2022, doi: 10.1021/acsearthspacechem.2c00052.

[62] X. Guo *et al.*, “Thermodynamics of formation of coffinite, USiO4,” *Proc. Natl. Acad. Sci.*, vol. 112, no. 21, pp. 6551–6555, 2015, doi: 10.1073/pnas.1507441112.

[63] C. Frondel, “Hydroxyl substitution in thorite and zircon,” 1953.

[64] L. R. Stieff, T. W. Stern, and A. M. Sheerwood, “Coffinite, A uranous Silicate with Hydroxyl subsitution: A New Mineral,” *Am. Mineral.*, vol. 41, no. 9–10, pp. 675–688, 1956, doi: 10.3133/tei538.

[65] A. C. Strzelecki *et al.*, “Thermodynamics of CeSiO4: Implications for Actinide Orthosilicates,” *Inorg. Chem.*, vol. 59, no. 18, pp. 13174–13183, 2020, doi: 10.1021/acs.inorgchem.0c01476.

AUTHOR INFORMATION

Corresponding authors

*N. D.: phone. +33 4 66 33 92 05; e-mail. nicolas.dacheux@umontpellier.fr

ORCID

Thomas Barral: 0000-0002-2730-7219

Paul Estevenon: 0000-0001-8517-4744

Yann Chanteau:

Thibault Kaczmarek: 0000-0003-4559-3615

Andrew Strzelecki: 0000-0003-3928-9422

Denis Menut: 0000-0001-8657-3333

Eléonore Welcomme: 0000-0002-3758-6717

Stéphanie Szenknect: 0000-0003-3691-3621

Philippe Moisy: 0000-0002-9331-0846

Xiaofeng Guo: 0000-0003-3129-493X

Nicolas Dacheux: 0000-0003-1636-1313

Notes

The authors declare no competing financial interest.

ACKNOWLEDGMENTS

The authors would like to thank Renaud Podor and Joseph Lautru (from ICSM) for supporting SEM experiments. Andrew C. Strzelecki and Xiaofeng Guo acknowledge the supports by the National Science Foundation (NSF), Division of Materials Research, under award No. 2144792